Multi-Input Multi-Output Repetitive Control Theory

And

Taylor Series Based Repetitive Control Design

Kevin Xu

Submitted in partial fulfillment of the
Requirement for the degree of
Doctor of Philosophy
In the Graduate School of Arts and Sciences

COLUMBIA UNIVERSITY

2012

ABSTRACT

Multi-Input Multi-Output Repetitive Control Theory And

Taylor Series Based Repetitive Control Design

Kevin Xu

Repetitive control (RC) systems aim to achieve zero tracking error when tracking a periodic command, or when tracking a constant command in the presence of a periodic disturbance, or both a periodic command and periodic disturbance. This dissertation presents a new approach using Taylor Series Expansion of the inverse system z-transfer function model to design Finite Impulse Response (FIR) repetitive controllers for single-input single-output (SISO) systems, and compares the designs obtained to those generated by optimization in the frequency domain. This approach is very simple, straightforward, and easy to use. It also supplies considerable insight, and gives understanding of the cause of the patterns for zero locations in the optimization based design. The approach forms a different and effective time domain design method, and it can also be used to guide the choice of parameters in performing in the frequency domain optimization design.

Next, this dissertation presents the theoretical foundation for frequency based optimization design of repetitive control design for multi-input multi-output (MIMO) systems. A comprehensive stability theory for MIMO repetitive control is developed. A necessary and sufficient condition for asymptotic stability in MIMO RC is derived, and four sufficient conditions are created. One of these is the MIMO version of the approximate monotonic decay condition in SISO RC, and one is a necessary and sufficient condition for stability for all possible disturbance periods.

An appropriate optimization criterion for direct MIMO is presented based on minimizing a Frobenius norm summed over frequencies from zero to Nyquist. This design process is very tractable, requiring only solution of a linear algebraic equation. An alternative approach reduces the problem to a set of SISO design problems, one for each input-output pair. The performances of the resulting designs are studied by extensive examples. Both approaches are seen to be able to create RC designs with fast monotonic decay of the tracking error.

Finally, this dissertation presents an analysis of using an experiment design sequence for parameter identification based on the theory of iterative learning control (ILC), a sister field to repetitive control. This is suggested as an alternative to the results in optimal experiment design. Modified ILC laws that are intentionally non-robust to model errors are developed, as a way to fine tune the use of ILC for identification purposes. The non-robustness with respect to its ability to improve identification of system parameters when the model error is correct is studied. It is demonstrated that in many cases the approach makes the learning particularly sensitive to relatively small parameter errors in the model, but sensitivity is sometimes limited to parameter errors of a specific sign.

Contents

List of Figures

Acknowledgements

I am greatly indebted to my research advisor Professor Richard W. Longman, who introduced me to the fields of Repetitive Control and Iterative Learning Control. His expertise has navigated me through many challenges in my research in these fields. He has always provided candid advice and deep insight during our weekly meetings, either in person or via Skype. I enjoyed every minute of these meetings. He is an excellent teacher and mentor, both on research and on life in general. It would be impossible to finish this dissertation without his encouragement and supervision.

I am also very grateful to Professor Minh Q. Phan at Dartmouth College, and Dr. Benjamas Panomruttanarug, a former member of the Control Systems Research Group at Columbia University, who is now a professor at King Mongkut's University in Thailand.

I would like to heartily thank my academic advisor Professor Dan Ellis, for always providing valuable academic guidance whenever I needed his help.

Chapter 1. Introduction

1.1 Repetitive Control Design for Single-Input Single-Output Systems

Repetitive control (RC) systems aim to achieve zero tracking error tracking a constant or periodic command in the presence of a periodic disturbance. For example, spacecraft often have vibration sources such as cryo pumps, momentum wheels, control moment gyros, etc. A slight imbalance in such rotating parts produces periodic vibrations of the vehicle that impair the capability of onboard scientific mission equipment, for example, fine pointing equipment such as a telescope, or experiments needing a good microgravity environment. Passive methods have limited ability to isolate the associated sensitive equipment from the vibrations of these internal moving parts. These considerations all push toward the use of active isolation methods. Active methods can use feedback control which again has limited performance. Feedback controllers have time constants for reaction to changes in the error and therefore do not keep up with a changing error signal. They also have phase lags that limit their response to a periodic disturbance even in steady state. The fundamental difficulty is that feedback control systems normally do not make use of knowledge that the error is a periodic function. They react to disturbances in the current period as if they have never seen them before. By taking advantage of this periodicity information, repetitive control can in theory completely eliminate the deterministic errors produced by periodic disturbances. At any time step, these methods look at the error in the last period of the disturbance and make adjustments to the command to a feedback control system in order to converge to zero error.

Early publications in repetitive control include [1-5]. The first of these was motivated to eliminate 60 Hz ripple in rectified AC voltage for particle accelerators. The simplest form of discrete time RC makes the equivalent of integral control action in classical control, with a

different integral for each phase of the disturbance period. This is used to adjust the command given to a feedback controller in order to eliminate the influence of the disturbance. In practice this repetitive control law is nearly always unstable, although it very often improves the error very substantially before the instability starts to appear. In order to make simple repetitive control work in practical applications, one needs to develop some kind of compensator design. Viewed from one perspective, an ideal compensator uses the inverse of the feedback transfer function in order to cancel the full system dynamics. Unfortunately, the inverses of discrete time transfer functions are almost always unstable which precludes using this approach. The process of producing a difference equation model from a differential equation fed by a zero order hold usually inserts zeros outside the unit circle making the inverse unstable [6]. The repetitive control design approach by Tomizuka, Tsao, and Chew [5] avoids this problem by aiming only to cancel the phase of the model, but does not aim to otherwise invert the model. Panomruttanarug and Longman [7] develop a method of designing FIR compensators that are optimized to match the steady state response of the system, aiming to invert the phase and the magnitude of the steady state frequency response. Thus the approach bypasses the instability issues by inverting the frequency transfer function instead of the transfer function itself.

The design approach in [7] minimizes a cost function in the frequency domain that aims to satisfy a sufficient condition for asymptotic stability of a repetitive control system as proved by Longman [8]. As suggested in the development in [8] and further investigated in [9], this frequency response condition is very close to being a necessary and sufficient condition for stability, and in fact it is a necessary and sufficient condition for stability if one asks that the repetitive control system be asymptotically stable for all possible disturbance periods [10], a result developed as part of the research for this dissertation (see Chapter 3). Reference [11] looks

at this condition from a different point of view showing how it is closely related to the settling time of the repetitive control system, and hence the cost function is approximately aiming to make the repetitive control transients decay quickly.

Implementation requires only taking a chosen number of error measurements from the previous period, multiplying by gains, and adding them up. It can be accomplished purely from input-output test data without the need for creating an analytical model [12]. The design method was seen to be very effective. And it produces various recognizable patterns of poles and zeros for the resulting compensator designs. For example, to handle the influence of zeros outside the unit circle, the design repeats the zero around a circle of roughly the same radial distance from the origin, with the zeros roughly evenly spaced around the circle. These patterns seemed somewhat mysterious, but the development in Chapter 2 of this dissertation explains their origin.

The approach in Chapter 2 (which is also published as [13]) is to develop a finite impulse response (FIR) compensator that mimics the inverse of the transfer function based on Taylor series. As an FIR compensator, it cannot be unstable. This creates a very simple approach that has considerable understanding and intuition associated with it. Each factor in the transfer function that cannot be cancelled by zeros introduced in the FIR compensator, are expanded in a Taylor series up to a chosen number of terms. A method is given to help decide how many terms to use.

When the method developed in Chapter 2 (also appearing in [13]), or the method of [7], is used in applications, one may need to introduce several extra aspects into the repetitive control design. In order to make the repetitive controller robust to unmodeled high frequency dynamics one introduces a zero-phase low-pass FIR filter [14, 15]. Robustness to model parameter uncertainty can be accomplished by use of a multiple model technique [16]. In order to better

handle the situation when the period is not an integer number of time steps one can introduce interpolation [17]. And various problems have multiple unrelated disturbances with different periods, as in a spacecraft with four control moment gyros. One can use the same compensator in a more complicated repetitive control structure as demonstrated in [18] and [19], which built upon the work of [20, 21]. In addition, the design approach in Chapter 2 is an alternative to that in Chapter 3 of this dissertation to address multiple-input, multiple-output problems, and this design approach may be substantially simpler.

1.2 Repetitive Control Design for Multi-Input Multi-Output Systems

1.2.1 Theory of Stability for Designing Repetitive Controllers in the Frequency Domain for Multi-Input Multi-Output Systems

The repetitive control literature is mostly limited to single-input single-output systems, and normally aims to eliminate all error of a given period, i.e. a fundamental and all harmonics. But in the real world, many applications require MIMO design methods. References [22, 23] perform experiments testing various control methods, using a Stewart platform as an isolation mount. A repetitive control law applied to such hardware looks back at the error observed in the previous period of the periodic disturbance, and adjusts the command to each of the six legs of the platform in such a way as to cancel the influence of the disturbance on any fine pointing equipment mounted on the platform. It is the purpose of Chapter 3 (giving results that also appear as [10]) of this dissertation to develop appropriate underlying theory, and to develop several approaches to extend this design to MIMO systems. Such a generalization allows one to apply the approach to the Stewart platform example, which needs six inputs and six outputs, without needing to find a way to mathematically decouple the problem. Reference [24] also

presents the mathematics for minimizing the Frobenius norm criterion, and treats robustification to parameter uncertainty using multiple models.

The organization of Chapter 3 is as follows. First the structure of the MIMO repetitive control problem is presented. In order to make the paper self contained, the mathematics used in Chapter 3 is developed from first principles. Properties of singular value decomposition of complex matrices are presented, relationships between several norms of matrices are given, and frequency response of MIMO systems is reviewed. Then the approximate monotonic decay condition that underlies the optimization used in the SISO RC design methods in [7,12,14,15,16,18,19] is generalized to MIMO systems. Reference [8] proves that this condition for SISO is a sufficient condition for asymptotic stability of SISO repetitive control systems, and this proof is generalized in this chapter. First a necessary and sufficient condition for asymptotic stability of MIMO repetitive control systems is developed, in analogy to the SISO development of such a condition in [8]. Then a set of four sufficient conditions for asymptotic stability is derived, including the approximate monotonic decay condition as one sufficient condition. Another of these conditions is important as a necessary and sufficient condition for asymptotic stability of a repetitive control system for all possible arbitrarily specified periods. All of these results are generalized to include a zero-phase low-pass learning cutoff filter for robustification. Then a method of designing compensators for MIMO repetitive control systems is developed that uses the SISO design method multiple times. And, finally one of the sufficient conditions based on a Frobenius norm, is presented as an appropriate MIMO optimization criterion, analogous to that used in the SISO case. This cost function has a unique minimum which can be found by solving a linear equation, making the design approach very tractable. Examples of this design approach are given in Chapter 4.

1.2.2 Repetitive Control Design Methods for Multi-Input Multi-Output Systems

The usual RC problem has one periodic disturbance, of a given period. This can have a fundamental frequency and many harmonics up to Nyquist frequency. The Control Systems Research Group led by Professor Longman at Columbia University and his coworkers in a series of publications has aimed to extend the theory to handle all the characteristics of the spacecraft vibration isolation problem. One generalization is to handle multiple-input, multiple-output problems. Chapter 3 develops the underlying theory of MIMO RC in some detail, some of which is also in Reference [24], which presents some design results and some robustification results. Reference [25] is a long journal article by Longman that presents the methods of each of the aforementioned references in a unified presentation. Chapter 4 [26] builds on this framework, and compares several different methods of designing MIMO RC systems. One approach handles the full system using a cost function, as suggested in Chapter 3 and Reference [24]. Another approach is able to reduce the MIMO problem to a set of SISO problems as suggested in Chapter 3. An important property of the design treated here is that they do not require one to have a mathematical model. Instead, it can directly use input-output data converted to frequency response information. The SISO design when applied to MIMO systems is seen to produce perhaps unexpected pole-zero locations in the system. It preserves the ability to pick the number of gains and the number of non-causal gains in the RC compensator individually for each input-output transfer function, and allows one to use inversion of the stably invertible part of the system as part of the compensator design. By comparison to SISO problems, the cost function when generalized to the MIMO problem loses some of its precision in addressing the actual stability boundary. Numerical investigation shows that both design methods are very effective in

producing asymptotically stable MIMO repetitive control systems that can learn fast and converge to zero tracking error.

1.3 Improved Parameter Identification Using Iterative Learning Control Design

The optimal experiment design field most often makes use of the Fisher information matrix, and develops methods to generate a sequence of inputs to experiments aiming to maximize a likelihood function [27-29]. This type of approach is based on stochastic modeling, and necessarily uses the current model in deciding how to optimize the next experiment. In Reference [30] a totally different approach is considered that also develops a sequence of experiments, each one based on the results of the previous one. But this time, use is made of iterative learning control (ILC) which is a relatively new field that develops iterative methods to adjust the input to a system aiming to converge to zero error in the system output following a desired trajectory [8, 31-35]. Both ILC and RC use methods of learning in repeating situations. In RC the command or disturbance is repeating in the sense that they are periodic functions. In ILC a control system is asked to perform the same operation repeatedly, each time starting from the same initial conditions. Much of the theory applies to both fields. A major objective in ILC is to find ways to make the decay of the errors robust to model errors. When using ILC for experiment design, one instead takes advantage of the lack of robustness to model errors, and lets the iterations progress, going unstable and creating larger and larger signals that are isolating and amplifying information concerning what is sufficiently wrong with the model to produce instability. Then system identification algorithms such as in [36-38] can be used on the data to correct the model.

There are very many approaches to designing iterative learning control laws. Since our experiment design objective is different than that of the ILC designer, we want a learning law

whose stability is particularly sensitive to model errors. The main purpose of Chapter 5 (also presented in [39]) is to develop ILC design approaches that deliberately make the stability of the iterations very sensitive to errors in the parameters of a model. Reference [30] uses an ILC design that is based on linear-quadratic optimal control theory, and this design is somewhat more robust to model errors than most. The approach used here starts from the phase cancellation ILC design method of Reference [34] and investigates several ways to modify it so that the stability robustness is small. The emphasis in Reference [30] was on model errors that relate to the order of the model, i.e. model errors that relate to missing dynamics such as parasitic poles or residual second order modes. In Chapter 5 we put the emphasis on model errors when the model order is correct but the model coefficients are inaccurate.

Chapter 2. Use of Taylor Series Expansion of the Inverse Model to Design FIR Single-Input Single-Output Repetitive Controllers

2.1 Repetitive Control Background

2.1.1 The Repetitive Control Problem Statement

The objective of a repetitive control system is to achieve zero error tracking a periodic command in the presence of a periodic disturbance when each has the same period, or zero error tracking a constant command in the presence of a periodic disturbance of known period, or zero error tracking a periodic command with no disturbance. Figure 2.1 shows the most common block diagram structure, where $R(z)$ is the repetitive controller, $G(z)$ is the closed loop feedback control system, $Y_D(z)$ is the desired trajectory, which can be either a periodic command or a constant command, and $V^*(z)$ is the periodic disturbance.
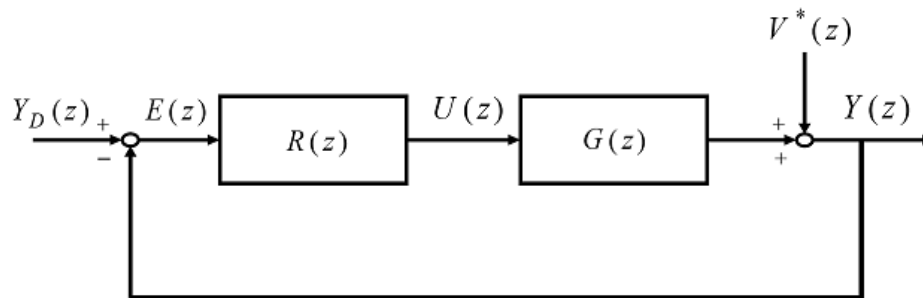
Figure 2.1 Repetitive control system

The diagram looks routine. What is unusual is that $G(z)$ represents the closed loop dynamics of a feedback control system whose command is $U(z)$, and the repetitive controller is adjusting this command with knowledge of the periodic nature of the desired trajectory $Y_D(z)$ and the periodic disturbance $V^*(z)$, aiming to converge to zero tracking error $E(z)$. The periodic disturbance can enter the hardware anywhere in the feedback control system loop, but there is always an

equivalent periodic disturbance that one could add to the output of the feedback controller, and can be modeled as $V^*(z)$ here. The repetitive control law takes the form

$$U(z) = R(z)E(z) = \left[\frac{\phi F(z)}{z^p - 1}\right] E(z) \tag{2-1}$$

where p is the number of time steps in a period, and $F(z)$ is the repetitive control compensator that is to be designed. By block diagram manipulation one can write the equivalent of a difference equation whose solution is the error as a function of time step for any command, disturbance, and initial conditions

$$\{1 - z^{-p}[1 - \phi G(z)F(z)]\}E(z) = (1 - z^{-p})[Y_D(z) - V^*(z)] \tag{2-2}$$

Because z^{-p} is a backward shift of one period, and $Y_D(z)$ and $V^*(z)$ are both periodic with this period, the right hand side is zero, and the difference equation is homogeneous.

$$\{1 - z^{-p}[1 - \phi G(z)F(z)]\}E(z) = 0 \tag{2-3}$$

Therefore the error will converge to zero as the time steps tend to infinity for all initial conditions if and only if all roots of the characteristic polynomial have magnitude less than unity, where the characteristic polynomial is given by the numerator of the curly bracket term after one puts everything over a common denominator.

2.1.2 The Model Inverse as a Compensator

In some respects the inverse of the system transfer function, $G^{-1}(z)$, is the ideal compensator $F(z)$. To see this, let $G(z) = K_G G_N(z)/G_D(z)$ and $F(z) = F_N(z)/F_D(z)$ where subscript N indicates numerator, subscript D indicates denominator, and K_G is a gain. Computing the numerator of the curly bracket produces $z^p G_D F_D - G_D F_D + K_G G_N F_N = 0$. If the

compensator is the system inverse, then $F_D = K_G G_N$ and $F_N = G_D$, and this produces the following characteristic polynomial

$$G_N(z)G_D(z)z^p = 0 \qquad (2\text{-}4)$$

The number p is equal to the number of time steps in a period can be very large. A big advantage of the system inverse as a compensator is that all of these roots have been placed at the origin. The characteristic polynomial of the feedback control system is $G_D(z) = 0$, and it is reasonable to assume that it is asymptotically stable with all roots inside the unit circle. The potentially serious problem is that the zeros of $G(z)$ are also roots of this repetitive control system characteristic polynomial, and the zeros can easily be outside the unit circle in which case this design approach fails.

2.1.3 Zeros Introduced in Conversion to Discrete Time

When a continuous time differential equation is fed by a zero order hold, one can write a difference equation that gives exactly the same output at the sample times. The corresponding z-transfer function has zeros introduced in this process. Provided the differential equation has fewer zeros than poles, then when a step input is applied for one time step, the output at the end of that step will be not zero (unless one is using a sample rate that is sufficiently low to have serious aliasing problems). This implies that the number of zeros in the z-transfer function will generically be one less than the number of poles, independent of how many zeros there were in the continuous time system (less than the number of poles). The number of zeros introduced is the pole excess minus one, where pole excess is the difference between the number of poles and the number of zeros in continuous time. Äström, Hagander, and Strenby [6] develop results showing where the zeros introduced by the discretization go as the sample time interval T tends

to zero. If one zero is introduced it approaches -1.00 (and one can show in various situations that it approaches from inside the unit circle). If two are introduced they approach -3.73 and -0. 278 asymptotically. If three are introduced they approach -9.89, -1.00, and -0.101. And if four are introduced they approach -23.2, -2.32, -0.431, and -0.0431. Note that asymptotically there is always a zero outside the unit circle if the pole excess in continuous time is three or more, and for such systems one cannot use the system inverse as a repetitive control compensator. Note also that asymptotically, each zero outside the unit circle is accompanied by a companion zero inside the unit circle at the reciprocal location.

2.1.4 The Frequency Response Optimization Criterion

One can rewrite equation (2-3) as

$$z^p E(z) = [1 - G(z)F(z)]E(z) \tag{2-5}$$

The z^p is a shift forward in time by one period, which is suggestive of interpreting the left hand side of the equation as the error in the next period, and the square bracket term as a transfer function from one period to the next. One will want to substitute $z = \exp(i\omega T)$ in this term to make a frequency transfer function. This is heuristic thinking, since frequency response is a steady state phenomenon, and we hope that the steady state error is zero. Nevertheless if one makes a quasi static assumption that the error does not change much from period to period, then one could consider that the component of the error at frequency ω will decay from one period to the next by the magnitude of the frequency transfer function, and that if all frequencies decay, the system will be stable

$$\left|1 - G(e^{i\omega T})F(e^{i\omega T})\right| < 1 \quad \forall \omega \tag{2-6}$$

This is an approximate monotonic error decay condition. The quasi static assumption needed here to obtain this condition is actually not a serious issue for reasonable size values of p, and as shown in Reference [11] the condition actually gives a very good indication of the decay of transients during the repetitive control process. Reference [8] establishes that this heuristically obtained condition is actually a sufficient condition for stability of the repetitive control system. Furthermore, Reference [8] develops a condition for the actual stability boundary, i.e. the system is asymptotically stable if and only if this new condition is satisfied. Then Reference [9] shows that the set of systems that can be asymptotically stable without satisfying (2-6) is very small in practical applications, and therefore the distinction between the two conditions is not usually of practical importance. Any SISO repetitive control system satisfying stability condition (2-6) will converge to zero error tracking any command of period p time steps, and will learn to completely eliminate the influence on the output of any periodic disturbance of period p. If one wants a compensator that produces asymptotic stability for all possible periods p, Reference [10] establishes that this condition is both necessary and sufficient, which will be presented in Chapter 3.

The repetitive control design method developed by Panomruttanarug and Longman in [7] picks the compensator in the form of an FIR filter

$$
\begin{aligned}
F(z) &= a_1 z^{m-1} + a_2 z^{m-2} + \cdots + a_m z^0 + \cdots + a_n z^{-(n-m)} \\
&= \frac{a_1 z^{n-1} + a_2 z^{n-2} + \cdots + a_n z^0}{z^{n-m}}
\end{aligned}
\tag{2-7}
$$

The implementation is simple, only requiring that one multiplies the measured errors from n time step in the previous period by a set of constants and add them up. The transfer function of the compensator has $n-1$ zeros that can be placed anywhere, and $n-m$ poles, all of which must be at the origin. The n coefficients are chosen to minimize a cost function, aiming to satisfy (2-6)

$$J = \sum_j [1 - G(e^{i\omega_j T})F(e^{i\omega_j T})]W_j[1 - G(e^{i\omega_j T})F(e^{i\omega_j T})]* \qquad (2\text{-}8)$$

where the asterisk indicates complex conjugate and the ω_j form a suitably chosen set of frequencies from zero to the Nyquist frequency. Hence, the FIR compensator aims to mimic the behavior of the steady state frequency response of the inverse system, and does not try to invert the transfer function itself.
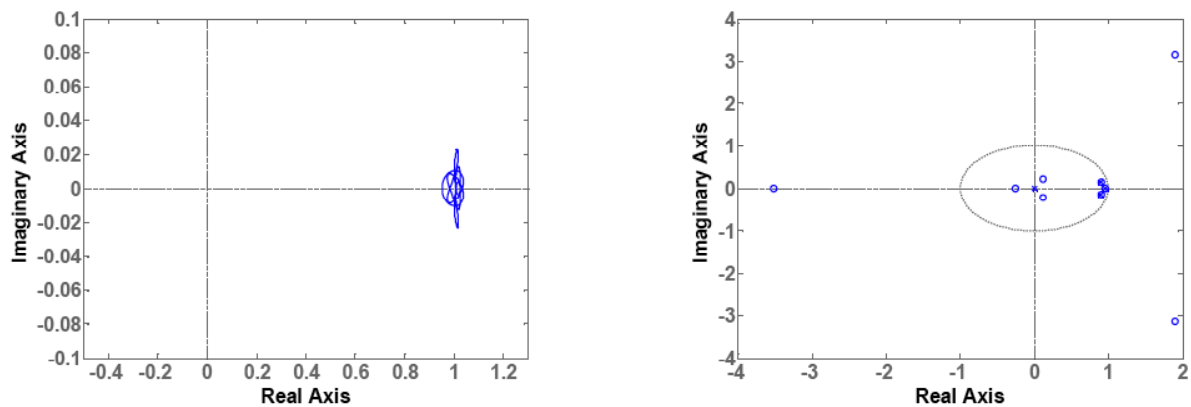
Figure 2.2 Polar plot of $G(e^{i\omega T})F(e^{i\omega T})$ for third order system using $n = 8, m = 5$ (left), and associated pole-zero map (right)

The approach can work very well. Reference [7] looks at a third order differential equation system fed by a zero order hold

$$G(s) = [a/(s+a)][\omega_o^2/(s^2 + 2\varsigma\omega_o s + \omega_o^2)] \qquad (2\text{-}9)$$

where $a = 1.4, \omega_o = 37\text{rad/sec}, \varsigma = 0.5$ and the sampling frequency in the zero order hold is 200 Hz. Using weights $W_j = 1$, a compensator with $n = 8, m = 5$ produced a plot of the real and imaginary parts of the product $G(e^{i\omega T})F(e^{i\omega T})$ as shown on the left in Figure 2.2. Thus the left hand side of (2-6) is the distance from +1 to the points on this plot and we see that this deviation from zero is small. Hence the FIR filter is a rather good approximation of the inverse of the frequency transfer function of the system using only 8 gains, and this makes a repetitive control

system that is both stable and learns very fast according to [11]. The right of Figure 2.2 shows the resulting pole-zero pattern. The zero order hold $G(z)$ has a zero outside the unit circle beyond -3, and a zero inside near the reciprocal location, and there are three poles that are the discrete time images of the poles in (2-9). The compensator puts zeros nearly on top of the three poles of the system. And it puts in two more zeros outside the unit circle very approximately evenly spaced around a circle of the radius of the system zero outside, and the same is done with the zero inside. One can change the value of m, and this will change the number of zeros introduced outside at the expense of the number introduced inside, or vice versa, and will result in a larger value for J. Increasing n produces better results with additional repeats of the original zeros around a curve that gets closer to being a true circle. Also, the cancellation of the system poles by zeros becomes more perfect.

To study how circularity is influenced by the distance from the origin to the zero, consider a system $G(z) = z + a$ with a zero on the negative real axis, and allow the compensator to have one zero. When the system zero is located at -1.1, the compensator zero is at 2.01, far from being on a circle of radius 1.1. If the system zero is put at 2, or 3, 4, … , 12, the compensator zero is located at 2.51, 3.34, 4.26, 5.21, 6.17, 7.15, 8.13, 9.12, 10.1, 11.1, 12.1, getting closer to being at the same radius as the zero gets further from the origin. When the system zero is at 20 or 100, the compensator zero is at 20.1 or 100, respectively. The radial distance also gets more uniform as the number of zeros allowed in the compensator is increased.

The design approach developed in section 2.4 supplies understanding of why these zero patterns accomplish their goal of imitating a pole to cancel a zero, by instead putting more zeros around a circle of the radius of the one whose influence is to be cancelled.

2.2 The Finite Impulse Response (FIR) and Infinite Impulse Response (IIR) Compensator Options

For purposes of this section, consider the case of a third order discrete time transfer function

$$G(z) = \frac{K_G(z - z_I)(z - z_O)}{(z - p_1)(z - p_2)(z - p_3)} \tag{2-10}$$

which could have come from (2-9). The poles are assumed all inside the unit circle, and there are two zeros introduced in the discretization, z_I inside the unit circle and z_O outside the unit circle. It is obvious how to generalize the process to include more zeros inside, more zeros outside, and more poles as needed. We consider two design choices.

2.2.1 Option A. $F(z)$ is an FIR Filter

The FIR filter (2-7) allows one to place zeros wherever one wants but all poles must be placed at the origin. The inverse of $G(z)$ can be written in the form

$$G^{-1}(z) = \left[\frac{(z - p_1)(z - p_2)(z - p_3)}{K_G} \right] \left[\frac{1}{z - z_I} \right] \left[\frac{1}{z - z_O} \right] \tag{2-11}$$

The first term can form some of the zeros of the FIR compensator (2-7). In order to handle the last two terms, Taylor series expansions are used which convert the terms with a denominator pole into an expansion in the numerator. The expansion is discussed in the following sections.

2.2.2 Option B. $F(z)$ is an IIR Filter

An alternative is to modify the form of the compensator (2-7) allowing one to introduce a pole that is not at the origin. Then we write (2-11) in the form

$$G^{-1}(z) = \left[\frac{(z - p_1)(z - p_2)(z - p_3)}{K_G(z - z_I)} \right] \left[\frac{1}{z - z_O} \right] \tag{2-12}$$

The pole in the first bracket is designed to cancel the zero of the system that is inside the unit circle. This cannot be done for the zero outside the unit circle, and hence it is expanded in a Taylor series as before. Thus everything that is stably invertible has been inverted, and what remains will be handled by expansion. Note that in implementation, instead of simply taking a linear combination of errors in the previous period in the RC control law, one needs to run a difference equation in real time.

2.3 A Basic Taylor Expansion Result

In order to address the Taylor series expansions desired in (2-11) and (2-12), consider the expansion

$$\frac{1}{1+\hat{z}} = 1 - \hat{z} + \hat{z}^2 - \hat{z}^3 + \cdots = \sum_{k=0}^{\infty} (-\hat{z})^k \tag{2-13}$$

The series is convergent provided $|\hat{z}| < 1$. Suppose that we approximate the right hand side by a finite series up through power r. Then the product of this approximation of a factor as on the right of (2-11) or (2-12) with the corresponding factor $(1+\hat{z})$ in the $G(z)$ that $F(z)$ multiplies will be approximately one. What is actually produced by this product is

$$[1+\hat{z}][1-\hat{z}+\hat{z}^2-\hat{z}^3+\cdots+(-\hat{z})^r] = 1 - (-\hat{z})^{r+1} \tag{2-14}$$

So the error in canceling the zero is given by $(-\hat{z})^{r+1}$. It is of interest to examine the roots of the polynomial on the right of (2-14), where it is clear that $-\hat{z}$ is any of the values of $r+1$ root of $+1$, i.e. write $1 = \exp(2\pi\ell)$ where ℓ can be any integer. Then the roots are

$$\hat{z} = -e^{i[2\pi\ell/(r+1)]} \tag{2-15}$$

Since one of the roots is $\hat{z} = -1$, the remaining roots are equally spaced around the unit circle with a separation angle of $2\pi/(r+1)$ radians between successive roots.

2.4 Taylor Expansions for Repetitive Control Zeros

For IIR option B above, we only need to create Taylor series expansions for the reciprocal of the system zeros outside the unit circle. For the FIR option A above we do this also for zeros inside the unit circle. These zeros can be zeros introduced by the discretization in which case they are always on the negative real axis. In addition one can have images of any zeros of the continuous time transfer function. These could be on the positive real axis, or they could be in complex conjugate pairs. And they could be outside the unit circle in which case one says that the system is non-minimum phase. Since the zeros introduced by the discretization are usually the ones that prevent one from using the system inverse as a compensator, we examine these in detail first, and then consider the other types of zeros.

2.4.1 Zeros on the Negative Real Axis Outside the Unit Circle

Consider $z_O = -a$ where $a > 1$ to make a zero outside the unit circle on the negative real axis. Then

$$\frac{1}{z - z_O} = \frac{1}{z + a} = \left(\frac{1}{a}\right)\left[\frac{1}{1 + (z/a)}\right] = \left(\frac{1}{a}\right)\left[\frac{1}{1 + \hat{z}}\right] \tag{2-16}$$

Thus we can use the expansion through power r as in (2-14) with $\hat{z} = z/a$. The series converges provided $|\hat{z}| < 1$, i.e. provided $|z| < a$. Our interest is in representing the frequency response which uses z on the unit circle, and hence this is within the radius of convergence. The resulting compensator introduces r roots around a circle of radius a. When combined with the original system zero at $-a$ gives $r+1$ roots evenly spaced around this circle.

2.4.2 Zeros on the Negative Real Axis Inside the Unit Circle

The FIR option A above wants to use the FIR filter structure to cancel the effects of a zero inside the unit circle on the negative real axis as usually occurs in discretization, $z_I = -a, 0 < a < 1$. Then

$$\frac{1}{z - z_I} = \frac{1}{z + a} = \left(\frac{1}{z}\right)\left[\frac{1}{1 + (a/z)}\right] = \left(\frac{1}{z}\right)\left[\frac{1}{1 + \hat{z}}\right] \qquad (2\text{-}17)$$

Pick a power r and again make the expansion of the last square bracket term through $\hat{z}^r$, this time with $\hat{z} = a/z$. The series converges provided $|z| > a$, and hence converges for z on the unit circle as needed. Note however that this series supplies poles at the origin. To illustrate this, consider $r = 2$, in which case the expansion becomes

$$1 - \left(\frac{a}{z}\right) + \left(\frac{a}{z}\right)^2 = \frac{z^2 - az + a^2}{z^2} \qquad (2\text{-}18)$$

There is one zero inside the unit circle, the one being addressed by the compensator, and the compensator introduced $r = 2$ more in (2-18). It also puts two poles at the origin in (2-18) and one more from (2-17), making the number of zeros inside the unit circle match the number of poles inside the unit circle. This was established as a requirement in [7]. To find the phase angle in the frequency response one looks at z on the unit circle starting at the origin for DC and going to -1 for Nyquist frequency. Looking at $G(e^{i\omega T})F(e^{i\omega T})$, any zero on the real axis inside the unit circle $z - z_I$ starts with phase zero at DC and reaches a phase of $+180°$ at Nyquist. And any complex conjugate pair of zeros inside will combine to create $+360°$. The stability condition (2-6) cannot be satisfied if the phase of $G(e^{i\omega T})F(e^{i\omega T})$ goes beyond $\pm 90°$. Hence, one needs to supply enough poles at the origin to match the number of zeros inside the unit circle.

2.4.3 Zeros on the Positive Real Axis

Zeros on the negative real axis were treated separately because they are ubiquitous in digital systems. Zeros on the positive real axis are handled totally analogously. This time zeros outside the unit circle give $z - z_O = z - a$ where $z_O = +a, a > 1$, and the resulting $\hat{z} = -z/a$. And for zeros inside $0 < a < 1$ and $\hat{z} = -a/z$.

Note that when the system zero is on the negative real axis, then that zero is on the circle, and the r introduced zeros are evenly spaced around this circle of radius a at angle intervals of $2\pi/(r+1)$ starting from the negative real axis. If the system zero is on the positive real axis one starts from the positive real axis. In the case of $r+1$ being even, both patterns will be identical, but when it is odd one is the mirror image of the other.

2.4.4 Complex Conjugate Zero Pairs

The expansions are still valid when the zero is complex and we wish to create an FIR approximation of

$$\left(\frac{1}{z - z_O}\right)\left(\frac{1}{z - z_O *}\right) \tag{2-19}$$

or similarly for z_I. One expands each separately picking the same value for r, and obtains for each zeros that are evenly spaced with interval $2\pi/(r+1)$ around a circle of radius $|z_O| = \rho$ starting at the zero location in (2-19).

2.5 Picking the Number of Compensator Zeros for Each System Zero

When there are multiple zeros at different radial distances from the origin, it is of interest to have some guidance in picking the number of repeats r for each zero. From equation (2-14) the error in cancellation of a zero using the Taylor expansion up through power r is given in

magnitude by $\left|\hat{z}\right|^{r+1}$. We are interested in z on the unit circle in satisfying (2-6). For real zeros

outside the unit circle and inside the unit circle, respectively, this becomes

$$\left|\frac{e^{i\omega T}}{a}\right|^{r+1} = \frac{1}{\left|a\right|^{r+1}} \tag{2-20}$$

$$\left|\frac{a}{e^{i\omega T}}\right|^{r+1} = \left|a\right|^{r+1} \tag{2-21}$$

and in the case of complex conjugate zeros one replaces a by ρ. It is natural to aim for the same

level of accuracy for canceling the effects of each zero by choice of the associated r. Suppose we

set this accuracy level to some number ε. For a zero outside, the number of repeats r should

satisfy $\varepsilon = 1/a^{r+1}$, and for inside it is $\varepsilon = a^{r+1}$. Solving for r in each case produces

$$r + 1 = \frac{\ln(1/\varepsilon)}{\ln a} \tag{2-22}$$

$$r + 1 = \frac{\ln \varepsilon}{\ln a} = \frac{\ln(1/\varepsilon)}{\ln(1/a)} \tag{2-23}$$

where a is greater than one in the first case, and less than one in the second. Of course r must be

picked as an integer, but these formulas can be used to make the error for each zero cancellation

be close. Note that as the zero location approaches the unit circle, the number of repeats r needed

for a given level of accuracy tends to infinity, as shown in Figure 2.3 which plots a from 1.025

to 5, and from 0.1 to 0.975.

An interesting additional property applies to the asymptotic zero locations. As the sample

time interval T tends to zero, for any zero introduced by discretization outside the unit circle,

there is a corresponding zero introduced inside the unit circle at the reciprocal location [6].

Comparing (2-22) and (2-23) we see that the number of repeats necessary for a given error level

is the same for zeros at reciprocal locations. It is noted by Panomruttanarug and Longman in [7]

that using the same number of repeats for each by adjusting the value of *m* in the FIR compensator (2-7) chosen to minimize the cost (2-8) seemed to produce the best results.
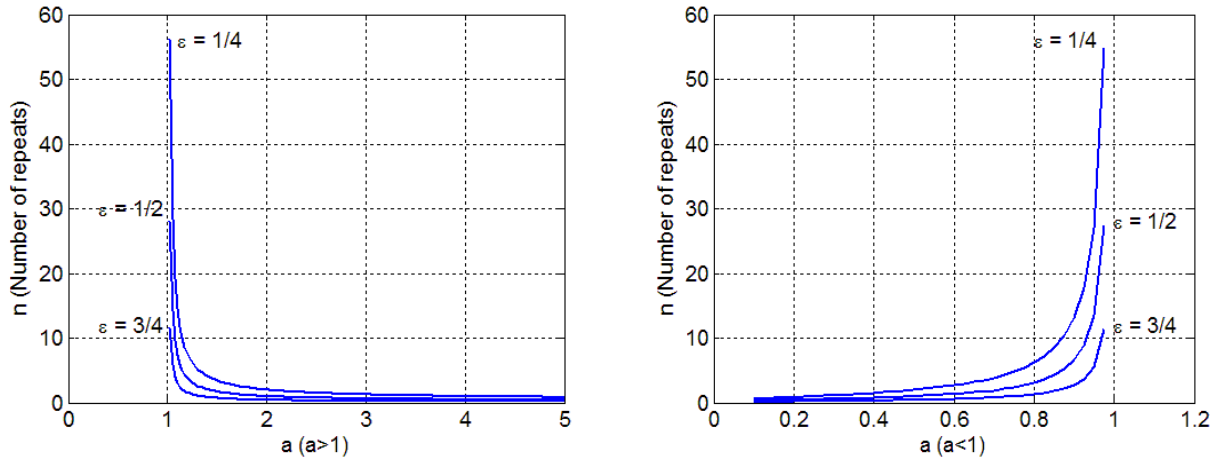
Figure 2.3 Number of repeats vs. zero location *a* for given error levels

2.6 Summary of the Design Process

Write the system transfer function in the form

$$G(z) = \frac{K_G G_{NI}(z) G_{NO}(z)}{G_D(z)} \tag{2-24}$$

where K_G is the gain, $G_D(z)$ are the poles of $G(z)$, $G_{NI}(z)$ is formed by the zeros inside the unit circle, and $G_{NO}(z)$ is formed by the zeros outside the unit circle. Pick an error level ε to use in deciding the number of repeats r to use for each factor. Then for the FIR compensator design approach

$$F(z) = F_A(z) F_I(z) F_O(z) \; ; \; F_A(z) = G_D(z)/K_G \tag{2-25}$$

The $F_I(z), F_O(z)$ contain the compensator factors for the zeros inside and the zeros outside the unit circle, respectively, given by

$$1 - \hat{z} + \hat{z}^2 - \hat{z}^3 + \cdots + (-\hat{z})^r \tag{2-26}$$

using the appropriate choice for $\hat{z}$ for the zero location, and using an appropriate choice for the value of r based on the chosen ε according to (2-22) and (2-23). The IIR design is obtain from

$$F(z) = F_B(z)F_O(z) \;\; ; \;\; F_B(z) = \frac{G_D(z)}{K_G G_{NI}(z)} \qquad (2\text{-}27)$$

2.7 Comments on Systems with Even Order Pole Excess in Continuous Time

Systems with even pole excess in continuous time that are fed by a zero order hold, when converted to discrete time introduce an odd number of zeros on the negative real axis, and asymptotically one of these zeros approaches -1 as the sample time interval T tends to zero. Under certain circumstances one can prove that the zero approaches -1 from inside the unit circle. Equations (2-22) and (2-23) indicate that as the zero approaches -1, the number of repeats needed for a given level of error in canceling the zeros effect, tends to infinity. Potentially, this can make it difficult to design compensators for even pole excess problems. One approach previously suggested is to introduce a first order continuous time filter into the system to produce an odd pole excess, eliminating any zero introduced near -1 [11]. Otherwise we have our choice of using the FIR design or the IIR design here. Each has its own potential advantages and disadvantages.

The IIR design is simple, it just introduces a pole underneath the zero near -1. As in equation (2-4), such a cancellation makes the root near -1 a root of the repetitive control system characteristic polynomial. And since it is near -1 it will have a solution to the homogeneous difference equation for the error (2-3) that is this root to the kth power at time step k. This part of the convergence will be slow. This may not be serious because this root is associated with Nyquist frequency, and it may be physically unlikely to have initial conditions that supply a sizable coefficient in front of this solution to the homogeneous equation. Of course this approach can only be applied if the zero near -1 is actually inside the unit circle. In the event that for the

non zero value of T being used, the zero is approaching -1 from outside, then one must use the FIR approach.

To help in the comparison, consider that the system of interest consists of nothing but a zero at the location $-a$,

$$G(z) = \frac{z + a}{1 + a} \qquad (2\text{-}28)$$

Equating $a^k = \exp(-\alpha kT) = [\exp(-\alpha T)]^k$ and solving for $1/\alpha = -T/\ln a$ gives the time constant associated with the envelope of decay of the solution associated with a compensator $F(z)$ equal to the inverse of $G(z)$.

At first one might think that the FIR approach avoids this issue of introducing a root that is near the stability boundary, by instead introducing a number r of additional zeros around the unit circle at this same radius. The actual result is to introduce $r + 1$ poles that are even closer to the unit circle stability boundary. Hence, of the two choices, putting a pole underneath the zero is preferred. To see this consider the sensitivity transfer function

$$S(z) = \frac{1}{1 + R(z)G(z)} \qquad (2\text{-}29)$$

where $R(z) = F(z)/(z^p - 1)$, and note that for the system in (2-28) and a less than unity, $F(z)G(z) = 1 - (-a/z)^{r+1}$. The denominator of the sensitivity transfer function is the characteristic polynomial of the repetitive control systems, which is

$$z^{p+r+1} = (-a)^{r+1} \qquad (2\text{-}30)$$

The magnitude of all roots are the same, and is equal to the $(r + 1)/(r + p + 1)$ root of a, and this is always closer to one than a itself. The conclusion is that one should place a pole underneath the zero instead of repeating the zero around a circle, when one has a zero approaching -1 from inside the unit circle.

2.8 Comparison of Frequency Response Based Compensator (Minimum Cost), Taylor Series Based Compensator, and Tomizuka Designs

It is of interest to examine the difference between the ways the frequency response based compensator design of [7] relates to the design produced here, and to the design method of [5]. Consider a system (2-28) consisting of just one zero located at -2, and no poles, and compare the resulting locations of the zeros introduced in the compensators by each method. The method of [5] introduces a zero at -1/2 and a pole at the origin, and normalizes for DC gain of unity.
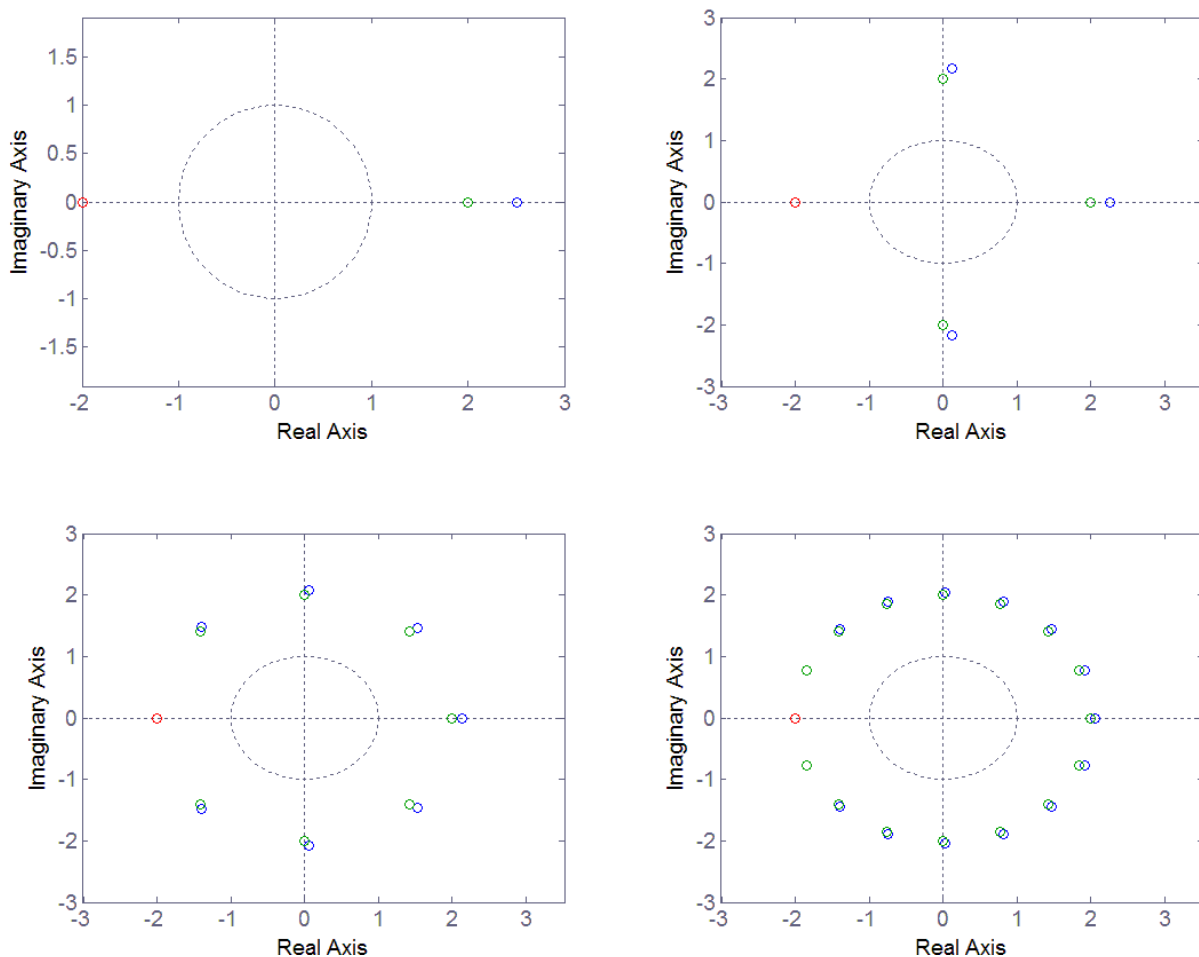
Figure 2.4 Zero locations of $G(z)F(z)$ when compensators are allowed to use one, three, seven, and fifteen zeros
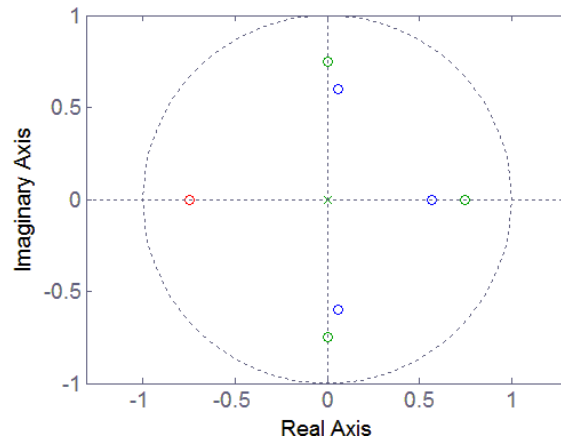
Figure 2.5 Zero locations of $G(z)F(z)$ when the system zero is inside the unit circle and compensators are allowed to use three zeros

Figure 2.4 examines the zero locations for the Taylor series and minimum cost methods. When the compensators are allowed to introduce only one extra zero, the results are in the upper left plot. Of course the Taylor series based design introduces its zero at +2, an example of evenly spaced around the circle of radius 2 about the origin. The zero introduced by the minimization in equation (2-8) with all weights equal to unity, is located at a larger radial distance as shown. The results when one allows the compensator to use 3 extra zeros are on the upper right. Again the radial distance to the frequency response based zeros are larger than 2, but this time we also see that the zeros are not quite evenly spaced, with the zeros near the imaginary axis being an angle somewhat less than 90°. The lower half of the figure shows what happens when one allows the compensators to use 7 and 15 zeros, and we see that as the number of zeros increases the difference between the two designs is converging to zero. Figure 2.5 shows that when the system zero is inside the unit circle the minimum cost design places zeros at smaller radial distance.

Consider the magnitude of the frequency response of $1 - G(z)F(z)$ given in Figure 2.6. According to [11] this is a good indicator of the amount of decay in each iteration for error

components at each frequency. We are again using the system in (2-28) with $a = 2$. The Taylor approach produces a horizontal line with zero slope, learning at all frequencies equally fast. The minimum cost approach learns slightly faster at low frequencies, and slightly slower at high frequencies. The method of Tomizuka [5] only aims to invert the system phase, and learns fast at very low frequencies, but quite slowly at higher frequencies. It is also of interest to compare the performance in terms of sensitivity transfer function which indicates how each design responds to disturbance frequency components that do not have the period being addressed.
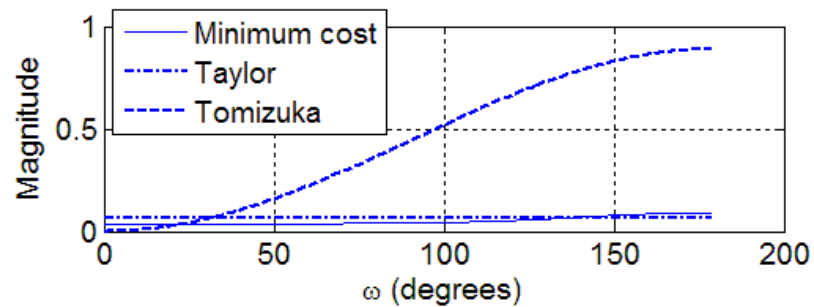
Figure 2.6 Magnitude frequency response of $1 - G(z)F(z)$

Figure 2.7 shows this when $p = 10$, $G(z)$ as in (2-28), with three zeros allowed in the compensator, and when the a in (2-28) equals 1.33, 1.05, and 0.75. For the cases when a is larger than one, the approach of Tomizuka is also shown (the approach cancels with a pole otherwise). This approach has smaller amplification between addressed frequencies at high frequency from the waterbed effect, because the learning is slow at these frequencies. We note that when a is near one, the Taylor approach has some high peaks between addressed frequencies that are not there in the minimum cost approach. This suggests that the minimum cost approach be used in such cases for better performance.
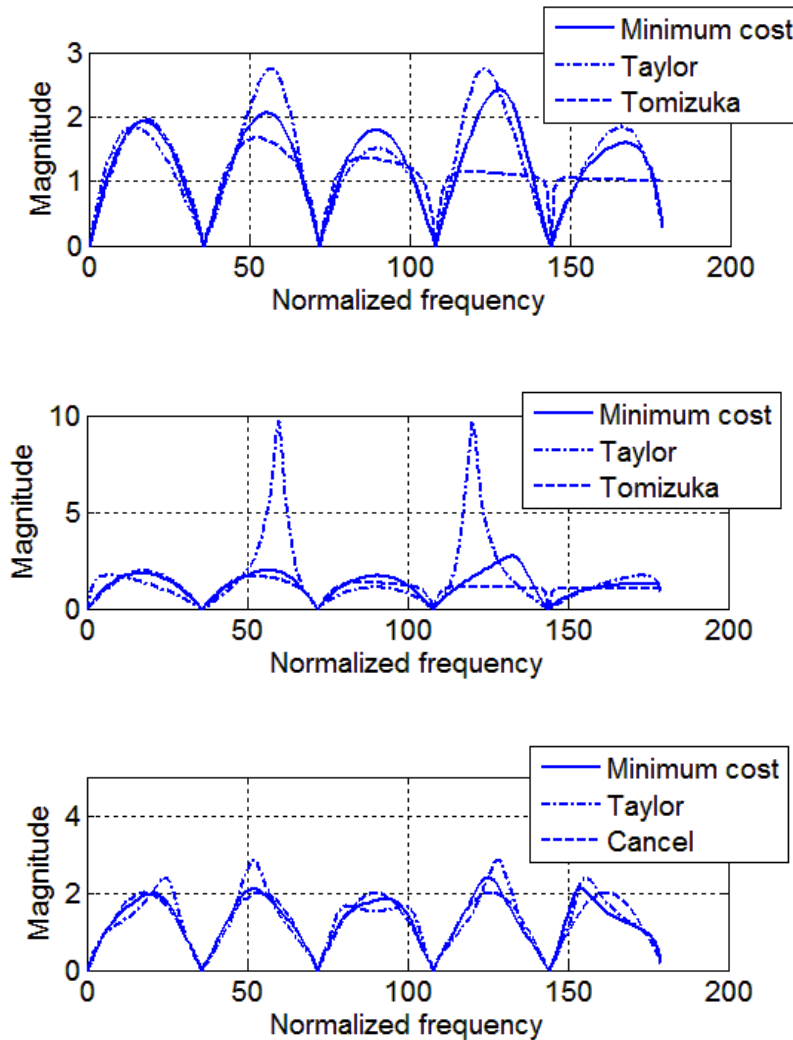
Figure 2.7 Sensitivity transfer functions magnitude frequency response for three repeats with *a* given as 1.33 (top), 1.05 (middle), and 0.75 (bottom)

2.9 Using Taylor Series Based Results to Guide Frequency Response Based Optimized Designs

The repetitive control design approach developed in this chapter has the advantage of being straightforward and simple. It also gives considerable insight. The design approach in [7] that picks the compensator (2-7) to optimize the cost function (2-8) could still produce better results because of the optimization involved. To use that method requires that one pick the values of n and m in (2-7) and this has been done by simply investigating a range of possibilities and

picking the one with the best behavior. In place of this process, one can make use of the results developed here to guide the choice.

For purposes of illustration, consider again the third order system (2-9). When fed by a zero order hold and sampled at any reasonable sampling rate, there is one zero introduced outside the unit circle and one introduced inside the unit circle, and the poles s_j are mapped to poles $z_j = \exp(s_j T)$ inside the unit circle in the equivalent z-transfer function. Using the FIR design method in this chapter, we can pick an error level ε and use (2-22) and (2-23) to pick values for the number of repeats to use for the zero inside and the zero outside: r_I, r_O. The compensator needs three zeros to cancel the system poles, so the power $n-1$ in the numerator of (2-7) is then equal to $3 + r_I + r_O$. We need the same number of zeros inside the unit circle as outside as noted above. The number of zeros inside the unit circle is 3 to cancel system poles, plus one system zero, plus the r_I zeros used in the Taylor expansion. Equating says that the number of poles we must introduce at the origin, the $n-m$ in equation (2-7), must equal $r_I + 1$. It is clear how to generalize this to handle higher order systems, more zeros inside, and more zeros outside.

Chapter 3. Design of Repetitive Controllers in the Frequency Domain for Multiple-Input Multiple-Output Systems

3.1 The Structure of the MIMO Repetitive Control Problem

Figure 3.1 shows the structure for repetitive control of a MIMO system. Normally, $G(z)$ represents the closed loop transfer function of a feedback control system, and $U(z)$ represents the command given this system. Instead, it can be just a plant that one wants to control. In either case it is assumed to be asymptotically stable, and to have the same number of inputs as outputs, denoted by q, so that $G(z)$ is a $q \times q$ matrix of transfer functions from each input to each output. The $Y_D(z), E(z), U(z), V(z), Y(z)$ are all q-dimensional column vectors, and $F(z), G(z)$ are both $q \times q$ transfer function matrices. The summation junctions in the diagram are element by element for each incoming vector.
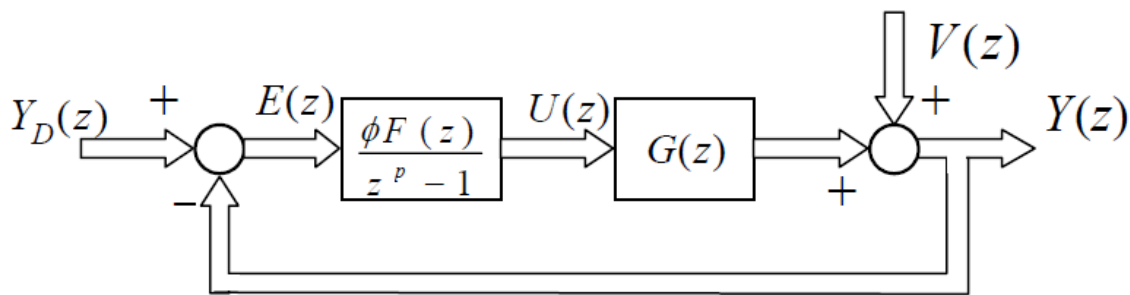
Figure 3.1 Block diagram of a MIMO repetitive control system

The $Y_D(z)$ is the desired output and $V(z)$ is any deterministic periodic disturbance whose influence is to be eliminated by the repetitive control action. Both desired output and the periodic disturbance are of period p time steps. Perhaps the predominant applications of RC are to the very important special case where the desired output is a constant, which is periodic with any period of interest, and the objective of the repetitive controller is to cancel the effects of a

periodic disturbance of known period. Periodic disturbances can appear anywhere in a feedback control loop. Wherever such disturbances appear, one can create a periodic disturbance to the output that produces the same influence on the output. This is done here, adding the disturbance to the output of $G(z)$ which usually represents a feedback control system.

The main objective of the repetitive control design process, is to create a compensator transfer function matrix $F(z)$ that stabilizes the repetitive control process so that it converges to zero error tracking the periodic command, in spite of the presence of the periodic disturbance. Since the compensator operates on old data, the design process has the opportunity to use non-causal designs, something very unusual in control system synthesis. The compensator is created as a set of FIR filters formed as a linear combination of errors observed at n different time steps in the previous period. The update of the command to the feedback control system is then made by adding to the command used one period back, a repetitive control gain ϕ times the filtered (i.e. compensated) error from the previous period:

$$U(z) = z^{-p}[U(z) + \phi F(z)E(z)] \tag{3-1}$$

$$
\begin{aligned}
F(z) &= a_1 z^{m-1} + a_2 z^{m-2} + \cdots + a_m z^0 + \cdots + a_{n-1} z^{-(n-m-1)} + a_n z^{-(n-m)} \\
&= [a_1 z^{n-1} + a_2 z^{n-2} + \cdots + a_m z^{n-m} + \cdots + a_{n-1} z^1 + a_n z^0]/z^{n-m}
\end{aligned}
\tag{3-2}
$$

The filter coefficients $a_1, a_2, \ldots, a_n$ are $q \times q$ gain matrices. The z^0 term in the filter multiplies the error one period back, $e(k-p)$, and terms are included both forward and backward from this time step. This compensator structure is the MIMO version of the very successful SISO repetitive control design in [7], which is given in equation (2-7).

It is the purpose of this chapter to do the following:

(1) To generate the MIMO equivalent of the heuristic monotonic decay condition.

(2) To develop the necessary and sufficient condition for asymptotic stability of the MIMO repetitive control system.

(3) To prove that the MIMO heuristic monotonic decay condition is a sufficient condition for asymptotic stability and hence convergence to zero error, and to establish additional sufficient conditions.

Note that all of the results of this chapter relating to necessary and sufficient conditions for stability, or sufficient conditions for stability apply for more general compensator structures. The form in equation (3-2) is only used when design methods are being discussed (in Chapter 4).

In order to present a complete self-contained development, we will start from first principles to develop all results.

3.2 Singular Value Decomposition of a Complex Matrix

We will need the singular value decomposition of a complex matrix which we review here. For simplicity, suppose that A is a square full rank matrix with complex valued entries. Consider the eigenvalue equation $A^H A v = \lambda v$, where λ is the eigenvalue and v is the associated eigenvector, H indicates the complex conjugate transpose. Assume that all the eigenvalues are unique. The magnitude of the eigenvector can be scaled up and down according to this equation, so let it be scaled such that $v^H v = 1$. Premultiplying the eigenvalue equation by v^H establishes that $\lambda = (Av)^H (Av) = \|Av\|_2^2$, indicating that all eigenvalues λ are real and non-negative. Since we assume that A is full rank, all eigenvalues are positive. Let σ_i be the square root of the i-th eigenvalue of A, $\sigma_i = \sqrt{\lambda_i}$, and define $\Sigma = diag(\sigma_1, \sigma_2, \cdots, \sigma_q)$. Also define matrix V to have the associated eigenvectors in the corresponding order. Packaging the eigenvalue equation for each eigenvalue into one matrix equation results in $A^H A V = V \Sigma^2$.

Consider the eigenvectors associated with two different eigenvalues λ_i and λ_j. For the two corresponding eigenvalue equations, pre-multiply the first by v_j^H and the second by v_i^H. Note that $v_j^H A^H A v_i$ is a scalar and hence is equal to its transpose, $v_i^H A^H A v_j$, and then take the difference of the two equations to obtain $(\lambda_i - \lambda_j) v_i^H v_j = 0$. Since the eigenvalues are distinct, we conclude that the eigenvectors are orthogonal. They are also of unit magnitude and hence $V^H V = I$, and $V^{-1} = V^H$.

Matrix U is defined such that A can be written as $A = U\Sigma V^H$, i.e. $U = AV\Sigma^{-1}$. Take the product of $U^H U$ and solve for $A^H A$ to obtain $A^H A = V\Sigma U^H U\Sigma V^H$. Equate this to the value obtained from the equation $A^H A V = V\Sigma^2$, and we conclude that $U^H U = I$, and $U^{-1} = U^H$. Examining AA^H and post multiplying by U produces $AA^H U = U\Sigma^2$. Comparing this to the equation $A^H A V = V\Sigma^2$, one concludes that the columns of U are the eigenvectors of AA^H and the σ_i^2's on the diagonal of Σ^2 are also the eigenvalues of this product.

The result is that complex matrix A can be written as $A = U\Sigma V^H$, where the conjugate transpose of U and V produces their inverse, and Σ is the diagonal matrix of real non-negative singular values. The analysis can be generalized to obtain the same form when the matrix is singular and when it has repeated eigenvalues and when it is not square.

Now consider the linear equation $Ax = b$, and substitute $A = U\Sigma V^H$ into the equation. Premultiply U^H to both sides gives $\Sigma V^H x = U^H b$. It can be written as $\Sigma \hat{x} = \hat{b}$, where $\hat{x} = V^H x$ and $\hat{b} = U^H b$. Note that $\|\hat{x}\|_2^2 = \|x\|_2^2$, and $\left\|\hat{b}\right\|_2^2 = \|b\|_2^2$. Then $\|b\|_2^2 = \left\|\hat{b}\right\|_2^2 = \hat{x}^H \Sigma^2 \hat{x} = \sigma_1^2 \hat{x}_1^2 + \sigma_2^2 \hat{x}_2^2 + \cdots \leq \sigma_{max}^2 (\hat{x}_1^2 + \hat{x}_2^2 + \cdots) = \sigma_{max}^2 \|x\|_2^2$, where $\sigma_{max}(A)$ is the largest singular value of A. Thus we conclude that

$$\|b\|_2 \leq \sigma_{max}(A)\|x\|_2 \tag{3-3}$$

3.3 Frobenius Norm, Maximum Singular Value, and Spectral Radius

The maximum singular value can be called the matrix norm induced by using the Euclidean norm for vector quantities, call it $\|A\|_2 = \sigma_{max}(A)$. One can also define the Frobenius norm of a matrix $\|A\|_F$ as the square root of the sum of the magnitudes squared of all terms in the matrix. This can be written as

$$\|A\|_F^2 = tr(A^H A) \tag{3-4}$$

Here tr indicates the trace of a matrix. Substituting the singular value decomposition of A into this equation results in $\|A\|_F^2 = tr[(V\Sigma)(V\Sigma)^H]$. Note that $tr(CC^H) = tr(C^H C)$ for any square matrix C. Therefore, $\|A\|_F^2 = tr[\Sigma V^H V\Sigma] = \sigma_1^2 + \sigma_2^2 + \cdots$ which is clearly greater than or equal to σ_{max}^2. We conclude that

$$\|A\|_F \geq \|A\|_2 \tag{3-5}$$

Hence, if $\|A\|_F < 1$ then $\|A\|_2 < 1$.

Now consider the spectral radius, $\rho(A)$, the largest magnitude of any eigenvalue of A. Apply equation (2-3) to the eigenvalue equation $Ax = \lambda x$ so that $b = \lambda x$. Then

$$\sigma_{max}(A)\|x\|_2 \geq \|\lambda x\|_2 = |\lambda|\|x\|_2 \tag{3-6}$$

This establishes the ordering

$$\|A\|_F \geq \sigma_{max}(A) \geq \rho(A) \tag{3-7}$$

3.4 Frequency Response of a MIMO System

Consider the MIMO system $G(z)$ written in state variable form

$$x(k + 1) = Ax(k) + Bu(k)$$

$$y(k) = Cx(k)$$

(3-8)

which is related to the transfer function form according to

$$G(z) = C(zI - A)^{-1}B$$

(3-9)

Suppose that the input is a general input of frequency ω given as

$$u(k) = \begin{bmatrix} \alpha_{I1} \cos(\omega kT + \beta_1) \\ \alpha_{I2} \cos(\omega kT + \beta_2) \\ \vdots \\ \alpha_{Iq} \cos(\omega kT + \beta_q) \end{bmatrix}$$

(3-10)

where each component is a sinusoid of arbitrary amplitude and phase. The j-th entry can be written as

$$\alpha_{Ij} \cos(\omega kT + \beta_j) = \frac{1}{2}\alpha_{Ij}e^{i\beta_j}e^{i\omega kT} + \frac{1}{2}\alpha_{Ij}e^{-i\beta_j}e^{-i\omega kT}$$

(3-11)

Define

$$\bar{u} = \begin{bmatrix} \alpha_{I1}e^{i\beta_1} \\ \alpha_{I2}e^{i\beta_2} \\ \vdots \\ \alpha_{Iq}e^{i\beta_q} \end{bmatrix}; \qquad \bar{\alpha}_I = \begin{bmatrix} \alpha_{I1} \\ \alpha_{I2} \\ \vdots \\ \alpha_{Iq} \end{bmatrix}$$

(3-12)

so that

$$u(k) = \frac{1}{2}\bar{u}e^{i\omega kT} + \frac{1}{2}\bar{u}^*e^{-i\omega kT}$$

(3-13)

Superposition allows us to find the steady state response of the system to input (3-10) by finding the response to the input $u(k) = \bar{u}e^{i\omega T}$, taking the complex conjugate of the response, adding the two together, and dividing by 2. Note that $\bar{u}^H\bar{u} = \bar{\alpha}_I^T\bar{\alpha}_I = \|\bar{\alpha}_I\|_2^2$, which is the square of the Euclidean norm of the amplitudes of the input signal. Look for a solution of the form $x(k) = \bar{x}e^{i\omega kT}$, $y(k) = \bar{y}e^{i\omega kT}$ and obtain the equation

$$\bar{y} = C[(e^{i\omega T})I - A]^{-1}B\bar{u}$$
$$\bar{y} = G(e^{i\omega T})\bar{u}$$

(3-14)

and corresponding solution

$$y(k) = \frac{1}{2}\bar{y}e^{i\omega kT} + \frac{1}{2}\bar{y}*e^{-i\omega kT}$$

(3-15)

As in the case of the input amplitudes in $\bar{\alpha}_I$, we define an output amplitude column vector $\bar{\alpha}_O$

and note that $\bar{y}^H\bar{y} = \bar{\alpha}_O^T\bar{\alpha}_O = \|\bar{\alpha}_O\|_2^2$. Apply the result in equation (3-3) to equation (3-14) to

obtain for any frequency ω

$$\|\bar{\alpha}_O\|_2 \leq \sigma_{max}(G(e^{i\omega T}))\|\bar{\alpha}_I\|_2$$

(3-16)

This bounds the Euclidean norm of the amplitudes of the outputs in terms of the norm of the

amplitudes of the inputs and the maximum singular value of the frequency transfer function

matrix. To make a bound over all frequencies from zero to Nyquist frequency, we can also write

$$\|\bar{\alpha}_O\|_2 \leq \max_\omega\left[\sigma_{max}(G(e^{i\omega T}))\right]\|\bar{\alpha}_I\|_2$$

(3-17)

3.5. Heuristic Monotonic Decay Condition for MIMO Repetitive Control Systems

To obtain the MIMO approximate monotonic decay condition, we imitate the

development of equations (2-3) and (2-5) for the MIMO case. This results in

$$\{z^pI - [I - \phi G(z)F(z)]\}E(z) = (z^p - 1)[Y_D(z) - V(z)]$$

(3-18)

The right hand side is zero, since both $Y_D(z)$ and $V(z)$ are periodic. Therefore,

$$z^pE(z) = [I - \phi G(z)F(z)]E(z)$$

(3-19)

Again we interpret the term in the square bracket $[I - \phi G(z)F(z)]$ as a transfer function from

one period to the next, and then look at its frequency response. Frequency response means steady

state frequency response. Again, this is heuristic thinking since $E(z)$ on each side of the equation

is actually the same function of time. If the system is stable, the error is zero when it gets to the

steady state. The thinking here assumes a quasi-static behavior in every period so that frequency response thinking can apply. The implication is that if we can make the amplitude of the frequency response of the transfer function matrix in the square bracket decrease at all frequencies, then all frequency components of the error will decrease every period, thus producing monotonic decay of error.

Applying equation (3-17) gives the MIMO approximate monotonic decay condition analogous to equation (2-6) as

$$\sigma_{max}\big[I - \phi G\big(e^{i\omega T}\big)F\big(e^{i\omega T}\big)\big] < 1 \quad \forall\, \omega \tag{3-20}$$

where $\sigma_{max}(A)$ denotes the largest singular value of a matrix A, which is also called the matrix norm induced by using the Euclidean norm for vector quantities, denoted as $\|A\|_2 = \sigma_{max}(A)$. In the next section, we will prove that this is a sufficient condition for asymptotic stability. Therefore, the assumptions made to develop the result here do not limit the use of the condition as something to satisfy to obtain stability, but the assumptions can limit the interpretation of the condition as an indicator of the decay rate each period.

3.6 Stability of MIMO repetitive control systems

3.6.1 A Necessary and Sufficient Condition for Asymptotic Stability

This section generalizes to MIMO the development of a necessary and sufficient stability condition for SISO repetitive control systems presented in References [8] and [40]. That result addresses the serious difficulty in using Nyquist stability criterion on repetitive control systems presented by the fact that for a period of p time steps, the open loop transfer function has p poles on the unit circle. And this requires the use of a Nyquist contour that goes around each of these poles making the approach prohibitive for most applications.

The words necessary and sufficient for asymptotic stability can be rephrased to say that the repetitive control system will converge to zero tracking error for a periodic command and periodic disturbance of period p time steps, for *all* initial conditions, if and only if the condition derived here is satisfied. We make the following assumptions about the repetitive control system:

(1) It has the structure given in Figure 3-1. The compensator $F(z)$ does not need to have the form given in equation (3-2), and it need not be causal.

(2) The denominator polynomial of $G(z)$ has all roots inside the unit circle. If it represents a feedback control system, this will automatically be satisfied.

(3) The denominator polynomial of $F(z)$ has all roots inside the unit circle. It seems natural to design an asymptotically stable compensator, and this condition is automatically satisfied when using equation (3-2). But we note that there are design approaches that do not guarantee this property [41].

(4) In order to be able to apply a repetitive control law, the period p must be large enough to make the repetitive controller causal. The number of time steps in a period is assumed to be large enough that all transfer function entries in $z^{-p}[I - \phi G(z)F(z)]$ have a higher degree polynomial in the denominator than the numerator. If one wants to use so many different time steps of error in (3-2) that this condition is violated, then one can make $2p$ the period used by the repetitive control law.

To start the development, rewrite equation (3-18) in the following forms

$$[z^{-p}(I - \phi G(z)F(z)) - I]E(z) = -(1 - z^{-p})[Y_D(z) - V(z)]$$

$$E(z) = -(1 - z^{-p})[z^{-p}(I - \phi G(z)F(z)) - I]^{-1}[Y_D(z) - V(z)] \qquad (3\text{-}21)$$

and note that

$$[z^{-p}(I - \phi G(z)F(z)) - I]^{-1} = \frac{\text{adj}[z^{-p}(I - \phi G(z)F(z)) - I]}{\det[z^{-p}(I - \phi G(z)F(z)) - I]}$$

where adj indicates the adjoint. Then (3-21) can be written as

$$\det[P(z)]E(z) = -(1 - z^{-p})\text{adj}[P(z)][Y_D(z) - V(z)] \tag{3-22}$$

$$P(z) = [z^{-p}(I - \phi G(z)F(z)) - I] \tag{3-23}$$

The determinant in (3-22) has both a numerator polynomial and a denominator polynomial. The numerator polynomial is the characteristic equation of the repetitive control system. If all roots of this polynomial are inside the unit circle, then the repetitive control system is asymptotically stable.
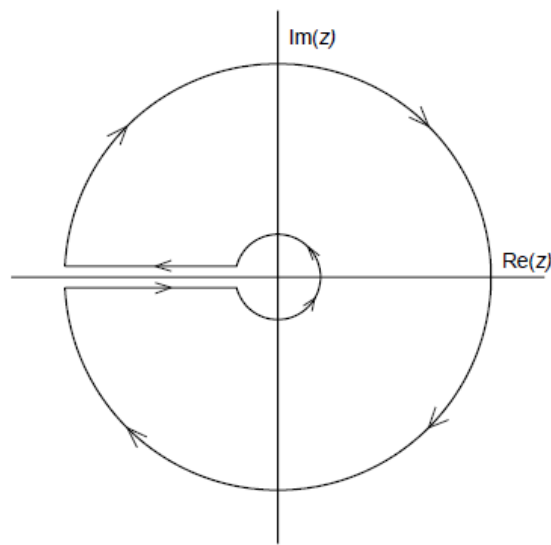
Figure 3.2 Nyquist contour for the digital control system

The principle of the argument that underlies the Nyquist stability criterion, examines the change in phase angle of the polynomial of interest as the value of z traverses a closed contour. Assume it is traversed once in a clockwise sense. Then each root of the polynomial inside the contour will cause the phase angle of the polynomial to have a net decrease in angle of 2π once the contour is traversed one time, and roots outside will produce no net change in the phase angle

of the polynomial. We use the Nyquist contour shown in Figure 3.2, which goes around the unit circle, goes out to infinity along a branch cut on the negative real axis, circles at infinity and comes back in along the branch cut. This contour includes everything outside the unit circle, and if there are no roots inside this contour then the system is stable. The assumptions above ensure that there are no roots on the contour. Rather than working to find the numerator polynomial, consider applying the method to $\det[P(z)]$. Under the assumptions above, all denominator roots are inside the unit circle, and hence outside the contour, and therefore they have no net effect on the phase change going around the contour.

Consider any z on the contour substituted into $P(z)$. This creates a matrix with complex numbers as entries, and any such matrix can either be diagonalized by a similarity transformation, or put into Jordan canonical form. Denote either of these forms by Λ as needed. Then

$$N^{-1}P(z)N = \Lambda \;\; ; \;\; P(z) = N\Lambda N^{-1} \tag{3-24}$$

The determinant of a product of matrices is the product of the determinants when each is defined. Since $NN^{-1} = I$, this implies that $\det N^{-1} = 1/\det N$. Hence,

$$\begin{aligned}
\det[P(z)] &= \det[\Lambda(z)] \\
&= \lambda_1(z)\lambda_2(z)\cdots\lambda_q(z) \\
&= r_1 e^{i\theta_1} r_2 e^{i\theta_2} \cdots r_q e^{i\theta_q} \\
&= (r_1 r_2 \cdots r_q)e^{i(\theta_1+\theta_2+\cdots+\theta_q)}
\end{aligned} \tag{3-25}$$

The repetitive control system is asymptotically stable if the angle $\theta_1 + \theta_2 + \cdots + \theta_q$ comes back to its original value when z goes once completely around the contour.

To simplify the process, define a new matrix

$$P*(z) = [z^{-p}(I - \phi G(z)F(z)] = P(z) + I \tag{3-26}$$

and note the relationship between the two determinants

$$\det[P*(z)] = \det[N^{-1}P*(z)N] = \det[N^{-1}P(z)N + N^{-1}N]$$
$$= \det[\Lambda + I] \tag{3-27}$$
$$= (\lambda_1(z)+1)(\lambda_2(z)+1)\cdots(\lambda_q(z)+1)$$

In this new form, the repetitive control system is stable if the angle of the line from the point -1 to the complex number $\det[P*(z)]$ relative to the positive real axis, comes back to its original value after z does one complete traversal of the contour. Making this shift assists in the evaluation of stability by allowing one to only consider the part of the contour that moves z around the unit circle. By the assumptions above, there are more poles than zeros in $P*(z)$, and therefore the part of the contour at infinity always maps to the origin. Also, the map from Nyquist frequency when $z = -1$ out to infinity along the branch cut on the negative real axis, and then coming back, forms a line from the point plotted for $z = -1$, which is on the real axis, to the origin and back. Hence, one does not need to expend effort to perform the mapping of these parts of the contour. What remains corresponds to plotting $z = \exp(i\omega T)$ which corresponds to using the frequency response. We state the result as a theorem.

Theorem 1: The repetitive control system shown in Figure 3-1, and satisfying the assumptions listed above, converges for all initial conditions to zero tracking error following a periodic command $Y_D(z)$ in the presence of a periodic disturbance $V(z)$, both of period p time steps, if and only if the plot of

$$\det[z^{-p}(I - \phi G(z)F(z))] \tag{3-28}$$

for $z = \exp(i\omega T)$, ωT going from zero to 2π, does not encircle the point -1. Equivalently, the angle made between the positive real axis direction and the line from -1 to the complex number represented by the above determinant, must come back to its original value (not modulo 2π) when z goes once around the unit circle.

3.6.2 Sufficient Conditions for Stability

   The stability condition in Theorem 1 gives a stability boundary that is dependent on the

period p of the command/disturbance in the repetitive control system. In most applications one

would want the repetitive control system to work for all periods that might occur, so a sufficient

stability condition that is independent of p would be desirable. The development of the SISO

stability condition in Reference [8] that is paralleled to generate the above theorem, eliminated

the need to have a contour that does an arc around p poles on the unit circle, but it leaves the

factor $z^{-p} = \exp(i\omega pT)$ whose phase spins very fast for typical periods. This can require very

fine sampling and complicate the effort to determine if the point -1 is encircled or not. As noted

in [40] and studied in [8] for the SISO case, the fast spin of the phase from this term means that

if the term it multiplies in (3-28) has magnitude larger than unity for even a small frequency

interval, the spin will make the plot encircle the point -1.

   We can generate a series of sufficient conditions for stability. For z on the unit circle, the

absolute value of the determinant in (3-28) satisfies

$$\left| \det[z^{-p}(I - \phi G(z)F(z))] \right| = \left| z^{-pq} \right| \left| \det[(I - \phi G(z)F(z))] \right| = \left| \det[(I - \phi G(z)F(z))] \right| \qquad (3\text{-}29)$$

Hence, if the determinant on the right in (3-29) is less than one in magnitude for all frequencies

up to Nyquist, then the point -1 cannot be encircled, and therefore this is a sufficient condition

for stability.

   When the determinant in the last expression is replaced by the product of the eigenvalues

of the matrix, and one uses the property in equation (3-25) for this problem, the right hand side

of (3-29) can be replaced by the product of the absolute values of the eigenvalues. If this product

is less than one, the repetitive control system must be asymptotically stable. Therefore, if the

maximum absolute value of any eigenvalue never exceeds unity, the system in asymptotically

stable, and this forms another, somewhat more restrictive sufficient condition. Using equation (3-7) establishes two more sufficient conditions, each more restrictive than the previous one. We can summarize these results in the following theorem that considers the magnitude of a determinant, the spectral radius, the maximum singular value, and the Frobenius norm.

Theorem 2: The repetitive control system shown in Figure 3.1, and satisfying the assumptions listed above, converges for all initial conditions to zero tracking error following a periodic command $Y_D(z)$ in the presence of a periodic disturbance $V(z)$, both of period p time steps, if any one of the following conditions is satisfied

$$\left|\det[(I - \phi G(e^{i\omega T})F(e^{i\omega T}))]\right| < 1 \ \forall \ \omega \tag{3-30}$$

$$\rho(I - \phi G(e^{i\omega T})F(e^{i\omega T})) < 1 \ \forall \ \omega \tag{3-31}$$

$$\sigma_{\max}(I - \phi G(e^{i\omega T})F(e^{i\omega T})) < 1 \ \forall \ \omega \tag{3-32}$$

$$\left\|I - \phi G(e^{i\omega T})F(e^{i\omega T})\right\|_F < 1 \ \forall \ \omega \tag{3-33}$$

$$tr[(I - \phi G(e^{i\omega T})F(e^{i\omega T}))(I - \phi G(e^{i\omega T})F(e^{i\omega T}))^H] =$$
$$tr[(I - \phi G(e^{i\omega T})F(e^{i\omega T}))^H (I - \phi G(e^{i\omega T})F(e^{i\omega T}))] < 1 \ \forall \ \omega \tag{3-34}$$

Each condition is a sufficient condition for asymptotic stability, with each equation being more restrictive than the previous equation, except that (3-33) and (3-34) are equivalent. Note that equation (3-33) says that the approximate monotonic decay condition (3-20) is a sufficient condition for asymptotic stability. Condition equation (3-32) is one that is particularly important to satisfy, because it not only guarantees asymptotic stability and convergence to zero error, it is also an approximate condition to enforce monotonic decay of the error during the convergence based on Reference [42]. Based on the logic used to develop (3-30) we can make the following stronger statement.

Theorem 3: A repetitive control system satisfying Theorem 1 converges to zero error for all possible periods *p*, and for all possible initial conditions, if and only if condition (3-30) is satisfied.

3.6.3 Robustification Using a Zero Phase Low Pass Filter

In designing a repetitive control system using a model, one would normally aim to create a compensator $F(z)$ that makes the system satisfy one of the above sufficient conditions for stability. In practice, it is difficult to have a model that maintains accuracy all the way to Nyquist frequency, while the repetitive control objective aims to converge to zero error for not only the fundamental frequency of period *p*, but also for all harmonics up to Nyquist frequency. As a result, parasitic poles or unmodeled high frequency dynamics can easily destabilize a repetitive control system in application to the real world [40]. References [14,15] develop methods of designing a scalar FIR filter of the same form as equation (3-2) that cuts off the learning process at high frequencies. In most applications, the cutoff frequency of the filter would be adjusted in hardware, since it is only by observing the behavior of the hardware that one knows what frequencies are too poorly represented in the design model to be learned.

Denote such a zero phase low pass filter by $H(z)$, which is a scalar function. When multiplied by a matrix, it signifies that all components are being filtered. Filtering all components of the signal to be applied to the system, creates the following repetitive control law, and repetitive control transfer function for Figure 3.1

$$U(z) = z^{-p} H(z)[U(z) + \phi G(z)F(z)E(z)]$$

$$U(z) = \frac{\phi H(z)F(z)}{z^p - H(z)} \tag{3-35}$$

In order to assess stability, we make this change and follow it through the development of the above theorems. Equation (3-22) is modified by having the factor $(1 - z^{-p})$ on the right hand side replaced by $(1 - z^{-p}H(z))$. This means that above the filter cutoff frequency, the right hand side of the difference equations is no longer zero. Hence, there can be a nonzero particular solution. If the repetitive control system is asymptotically stable, the transients will decay to zero leaving one with this solution. The $P(z)$ in (3-22) is replaced by

$$P(z) = [z^{-p}H(z)(I - G(z)F(z)) - I]$$

Equation (3-26) is modified to $P*(z) = z^{-p}H(z)(I - G(z)F(z))$. Assumption (4) is modified to ask that p be large enough that all transfer functions in this matrix $P*(z)$ have more poles than zeros. Then we can state the following Theorem.

Theorem 4: Under the above modified assumptions, Theorems 1, 2, and 3 apply to the repetitive control law (3-35) provided the term

$$z^{-p}[I - \phi G(z)F(z)] \tag{3-36}$$

is replaced by

$$z^{-p}H(z)[I - \phi G(z)F(z)] \tag{3-37}$$

in equations (3-28), (3-30), (3-31), (3-32), (3-33), and (3-34), and convergence to zero error is replaced by asymptotic stability of the solution of the homogeneous equation (i.e. all solutions of the homogeneous difference equation governing the repetitive control system, converge to zero as the time steps tends to infinity).

Chapter 4. Multiple-Input Multiple-Output Repetitive Control Design Methods

In this chapter, we develop a methodology to design the MIMO compensator using multiple SISO designs, and generalize the cost function (2-8) for SISO RC design to address MIMO problems [10, 26].

4.1 A SISO Approach to Designing MIMO Repetitive Control Systems

4.1.1 Analytical Approach with a Transfer Function Model

From equation (3-28) and (3-30) it is clear that designing the compensator $F(z)$ so that its frequency response closely matches that of $G^{-1}(z)$ will produce stability. Reference [7] shows that for a SISO system, it is not very effective to optimize the difference between the two functions (optimization function J_1 of that reference) by adjusting the coefficients in equation (3-2). Instead, one should try to make the product $G(z)F(z)$ look as much like one as possible, according to the optimization criterion equation (2-8). This section offers a method of using the SISO design process from equation (2-8) to handle the MIMO problem.

For simplicity, consider the case of two inputs, two outputs so that $q = 2$. There are q^2 transfer functions in $G(z)$, and we can design q^2 compensators for $F(z)$. Our interest is to make $F(z)$ look like $G^{-1}(z)$ in terms of frequency response, where

$$G(z) = \begin{bmatrix} g_{11}(z) & g_{12}(z) \\ g_{21}(z) & g_{22}(z) \end{bmatrix}$$

$$G^{-1}(z) = \frac{1}{g_{11}(z)g_{22}(z) - g_{12}(z)g_{21}(z)} \begin{bmatrix} g_{22}(z) & -g_{12}(z) \\ -g_{21}(z) & g_{11}(z) \end{bmatrix} = \begin{bmatrix} h_{11}(z) & h_{12}(z) \\ h_{21}(z) & h_{22}(z) \end{bmatrix}$$

(4-1)

Hence we would like to design the 1,1 component of $F(z)$, call it $f_{11}(z)$, to imitate

$$h_{11}(z) = \frac{g_{22}(z)}{g_{11}(z)g_{22}(z) - g_{12}(z)g_{21}(z)} \tag{4-2}$$

and analogously for the three other components. This makes four separate SISO design objectives, one for each component. Of course, as explained above, we do not want to directly match $f_{11}(z)$ with (4-2), but instead we want to make the product of $f_{11}(z)$ and the reciprocal of equation (4-2) look as close as possible to unity at all frequencies. Therefore, we make the following optimization criterion for design of $f_{ij}(z)$ of the form of the scalar version of equation (3-2)

$$J_{ij} = \sum_{k=0}^{N-1} \left\{ \left[1 - \left(h_{ij}(z) \right)^{-1} f_{ij}(z) \right] W_k \left[1 - \left(h_{ij}(z) \right)^{-1} f_{ij}(z) \right]^* \right\} \bigg|_{z=\exp(i\omega_k T)} \tag{4-3}$$

where $i = 1,2,\cdots,q$, $j = 1,2,\cdots,q$.

In the design process, one adjusts the values of n and m in equation (3-2) to find a design that makes these costs small. Each optimization problem simply requires the solution of a linear set of equations giving the compensator gains minimizing the cost. For this part of the design process, there is no requirement that the function multiplying the compensator component functions in the cost be stable. Note that each element of $G(z)$ will normally have a pole excess of one if it comes from feeding a differential equation with a zero order hold. And using this means that the reciprocal of (4-2) used in (4-3) is causal. After making a design for each entry in the compensator matrix, one then tests for stability of the design. One could of course use Theorem 1, but more likely one would want a design that works for all periods, and then one can check stability by Theorem 3. Of course, one can check the approximate monotonic decay condition (3-32), and if it is satisfied, then the system is stable. And the size of the maximum singular value is an approximate bound on the decay from one period to the next, according to the quasi-static thinking used in developing equation (3-20).

4.1.2 Computational Methods from Frequency Response Information

Equation (4-3) made use of some analytically developed expressions. When creating a program to perform the optimization, the process can be simplified. If one has an analytical expression for $G(z)$, for each of the round bracket entries in the jth term of the sum in cost functions like (4-3), one can numerically compute the matrix $G(e^{i\omega_j T})$, take its inverse, and then take the reciprocal of each entry to use in the cost. This simplification becomes increasingly important if q is not small.

One might not have an analytical expression. Reference [12] shows how one can use input-output data to generate the frequency response, as magnitude and phase change information. The same method can be used for a MIMO system. One can have the values of $G(e^{i\omega_j T})$ for each frequency, computed directly from input-output test data, and use this in equations like (4-3) to design the MIMO compensator, without ever developing a transfer function or differential equation model.

4.2 An Optimization Based Design Approach for MIMO Repetitive Control

The previous section performed a separate SISO repetitive control design for each component of the MIMO compensator. Now consider how one can formulate an appropriate cost function to deal directly with the MIMO problem. One might first ask to minimize the maximum value of the determinant in equation (3-28), since getting this value below unity ensures stability. Of course, it is perhaps better to use equation (3-30) to make the design independent of the value of the period p. And we could replace the maximum value, which creates difficult numerical minimization problems, by the sum of the magnitudes at a chosen set of frequencies from zero to Nyquist, producing

$$J = \sum_{j=0}^{N-1} \left\{ W_j \det\left[I - \phi G(z_j)F(z_j)\right] \det\left[I - \phi G(z_j)F(z_j)\right]* \right\} \bigg|_{z_j = \exp(i\omega_j T)} \tag{4-4}$$

Derivative information for minimizing this cost is obtainable. Taking the derivative with respect to any chosen scalar parameter in the coefficients in the $F(z)$ of equation (3-2), requires the derivative of the first determinant times the second, plus the first times the derivative of the second. And the derivative of a determinant with respect to a parameter α can be computed using

$$\frac{\partial}{\partial \alpha} \begin{vmatrix} c_{11} & c_{12} \\ c_{21} & c_{22} \end{vmatrix} = \begin{vmatrix} \partial c_{11}/\partial \alpha & c_{12} \\ \partial c_{21}/\partial \alpha & c_{22} \end{vmatrix} + \begin{vmatrix} c_{11} & \partial c_{12}/\partial \alpha \\ c_{21} & \partial c_{22}/\partial \alpha \end{vmatrix} \tag{4-5}$$

However, setting the derivative to zero would produce a set of equations that are polynomial in the many coefficients of the compensator, and is likely to have many local minima.

In place of minimizing (3-30) over the range of frequencies, one could consider using the spectral radius in (3-31). However, minimizing the magnitude of the largest eigenvalue of a general complex matrix is not an easy problem numerically, with particular difficulties in differentiability when decreasing the maximum eigenvalue makes it into a repeated eigenvalue. Minimizing the left hand side of (3-32) averaged over frequencies is a somewhat more tractable problem numerically. The σ_{max}^2 is again a maximum eigenvalue, but it is automatically real and positive, and it is associated with a matrix that is Hermitian, so that the eigenvector matrix always exists and has orthogonal rows and columns, even when there are repeated eigenvalues. Nevertheless, this is still a difficult problem numerically.

Using equation (3-34) as the basis for an optimization function, however, creates a quadratic cost whose unique minimum can be found by solving a linear algebraic equation, making this approach very tractable. This cost function maintains the simplicity of the SISO cost

(2-8) which also produces a set of linear equations to solve. To obtain this property in the MIMO case we have moved further from the criterion defining the necessary and sufficient stability boundary. In the SISO case, the cost used could be justified as optimizing not only for stability, but also for good transients, aiming to increase the learning speed of the repetitive controller. When shifting to using (3-34) instead of (3-32) we no longer have the interpretation of optimizing the speed of learning. But from equation (3-7), $\|A\|_F^2 \geq \sigma_{max}^2(A) \geq \rho^2(A) \geq 0$, by decreasing the Frobenius norm we are squeezing a bound on the approximate monotonic decay condition. Note that in the design process, we pick the number of gains used and which errors to include in the RC design when we pick n and m in equation (3-2). If the design that is minimizing the average of the square of the Frobenius norm succeeds in satisfying (3-34) then the design is table. But even if this condition is not satisfied, conditions (3-32), (3-31), or (3-30) might be satisfied, and this would imply stability. Hence, in creating the design one adjusts the parameters to get stability in one of these senses. And to aim for good learning transients, one can put extra emphasis on how small the left hand side of (3-32) becomes. Note that the left hand side of (3-32) for any frequency is an indicator of how fast that frequency decreases with periods. A design can still be practical if the left hand side gets larger than unity at high frequencies, in which case one needs to introduce a zero phase filter cutoff of the learning as discussed above, in order to stabilize the process.

The minimization problem using (3-34) can be formulated as follows. Write the compensator equation in the form

$$F(z) = M(z)\Phi \tag{4-6}$$

where

$$M(z) = \begin{bmatrix} z^{m-1}I & z^{m-2}I & \cdots & z^{-(n-m)}I \end{bmatrix}$$

$$\Phi = \begin{bmatrix} a_1^T & a_2^T & \cdots & a_n^T \end{bmatrix}$$

(4-7)

Then the cost function is written as

$$J = \sum_{j=0}^{N-1} W_j tr\left\{[I - G(z_j)M(z_j)\Phi]^H [I - G(z_j)M(z_j)\Phi]\right\}\bigg|_{z_j = e^{(i\omega_j T)}} + tr(\Phi^T R\Phi)$$

(4-8)

The last term is a penalty introduced to limit the size of the gains used in the compensator as discussed in [7]. Taking the derivative of the cost function with respect to the gain matrix Φ and setting the result to zero creates a linear set of equations to solve for these gains.

In order to conveniently find the derivative of J with respect to Φ we make use of some properties of the trace, and the derivative with respect to a matrix:

(i) First, $tr(AB) = tr(B^T A^T)$ for any matrices A and B. To see this, let the i,j components of these matrices be a_{ij} and b_{ij}. Then using the Einstein summation convention that sums over repeated subscripts, the i,k component of the product AB is given by $a_{ij}b_{jk}$, and the trace of the product is $a_{ij}b_{ji}$. Doing the analogous steps for $tr(B^T A^T)$ establishes the equality.

(ii) Define the derivative of a scalar $\bar{J}$ with respect to a matrix B as a matrix whose α, β component is $\partial \bar{J} / \partial b_{\alpha\beta}$.

(iii) Then $\partial[tr(AB)] / \partial B = A^T$. To see this note that $\partial[tr(AB)] / \partial b_{\alpha\beta} = \partial(a_{ij}b_{ji}) / \partial b_{\alpha\beta} = a_{\beta\alpha}$ since the derivative is zero except when $i = \beta$ and $j = \alpha$.

(iv) Also, $\partial[tr(B^T AB) / \partial B = (A + A^T)B$. The trace can be written as $b_{ik}a_{ij}b_{jk}$. Differentiating with respect to $b_{\alpha\beta}$ obeys the product rule, so that we can take the derivative of the first b_{ik} term times the rest, plus the first two terms times the derivative of b_{jk}. This produces $a_{\alpha j}b_{j\beta} + a_{i\alpha}b_{i\beta}$. When put back into matrix form one gets the result.

Let

$$\bar{J} = tr[(I - GM\Phi)^H (I - GM\Phi)]$$
$$= tr\{I - [(GM) + (M^H G^H)^T]\Phi + \Phi^T (M^H G^H GM)\Phi\}$$

(4-9)

then

$$d\bar{J} / d\Phi = -[(GM)^T + (M^H G^H)] + [(M^H G^H GM) + (M^H G^H GM)^T]\Phi$$

(4-10)

Introduce the summation in equation (4-8), the weight factor W_j, and the extra penalty term on large gains, and recognize that the result must be real so that imaginary parts must sum to zero, and one can produce the following solution to the optimization problem

$$\Phi = A^{-1}B$$

(4-11)

where this time A and B are given by

$$A = \sum_{j=0}^{N-1} W_j \left[\text{Re}(M^H(z_j)G^H(z_j)G(z_j)M(z_j)) + \text{Re}(M^H(z_j)G^H(z_j)G(z_j)M(z_j))^T \right] + 2R$$

(4-12)

$$B = \sum_{j=0}^{N-1} W_j \left[\text{Re}(G(z_j)M(z_j))^T + \text{Re}(M^H(z_j)G^H(z_j)) \right]$$

(4-13)

Reference [24] developed this result, and it discusses how to robustify the resulting design to model inaccuracies by picking the gains to minimize the cost function (4-8) written for a distribution of possible models or model parameters, and summed over this distribution.

4.3 An Example MIMO System

In order to study the comparison between the MIMO RC design approach of equation (3-33), and the multiple SISO design approach of the previous section, we consider the three mass system give in Figure 4.1. It is a two-input two-output system, $q = 2$. The system has three masses and three springs.
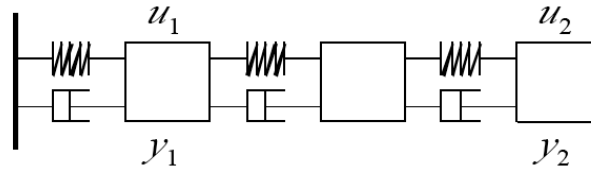
Figure 4.1 A three mass, two input, two output dynamic system

The continuous time differential equation for the system is

$$M\ddot{q} + N\dot{q} + Kq = Lu \tag{4-14}$$

where

$$M = \begin{bmatrix} m_1 & 0 & 0 \\ 0 & m_2 & 0 \\ 0 & 0 & m_3 \end{bmatrix}, \; K = \begin{bmatrix} K_1 + K_2 & -K_2 & 0 \\ -K_2 & K_2 + K_3 & -K_3 \\ 0 & -K_3 & K_3 \end{bmatrix}, \; L = \begin{bmatrix} 1 \\ 0 \\ 1 \end{bmatrix} \tag{4-15}$$

and the damping is taken to be proportional damping, which can be written in the form $N = 2\zeta\sqrt{K}$. The square root can be taken by diagonalizing matrix K, and taking the positive square root of each eigenvalue and converting back to original coordinates. The state variable form of the equation is

$$\dot{x}_c = A_c x + B_c u \tag{4-16}$$

$$x = \begin{bmatrix} q \\ \dot{q} \end{bmatrix}, \; A_c = \begin{bmatrix} 0 & I \\ -M^{-1}K & -M^{-1}N \end{bmatrix}, \quad B_c = \begin{bmatrix} 0 \\ L \end{bmatrix}, \; y = \begin{bmatrix} y_1 \\ y_2 \end{bmatrix} = \begin{bmatrix} 1 & 0 & 0 & 0 & 0 & 0 \\ 0 & 0 & 1 & 0 & 0 & 0 \end{bmatrix} x \tag{4-17}$$

The masses are all taken as unity, $m_1 = m_2 = m_3 = 1$. The spring constants are $K_1 = 20$, $K_2 = 60$, $K_3 = 100$, going from the spring connected to the wall, to the spring connected to the free mass at the end. For the proportional damping we consider three damping ratios ζ, given by 0.2, 0.1, and 0.01. Consider two input forces u_1 and u_2 at the first and the third mass as indicated (positive sense to the right), and the two outputs are the positions of the same two masses, y_1 and y_2 (positive sense to the right). The inputs are considered coming through zero order holds

sampling with a sample time interval of $T = 1/8$ s. From this we generate the discrete time state space model.

The desired trajectory for mass 1 next to the wall, and for mass 3 at the free end are given respectively as

$$y_{1D} = \sum_{i=1}^{5} \frac{1}{(i\omega_0)^2} \cos(i\omega_0 t), \ y_{2D} = \sum_{i=1}^{5} \frac{1}{(i\omega_0)^2} \sin(i\omega_0 t), \ \omega_0 = (2\pi)/(60T) \quad (4\text{-}18)$$

**4.4 Numerical Results Designing RC Using the Multiple SISO Method**

Results are generated using the multiple SISO design method of equation (4-3) with the weight factor set to unity, and using $n = 30$, a number chosen rather arbitrarily. The values of m were adjusted for best value, which was $m = 2$ for the diagonal elements of $F(z)$, and $m = 3$ for the off diagonal elements. Much smaller values of n also worked. And with $n = 10, m = 1$ does not produce singular values below unity for all frequencies, $m = 2$, 3, and 4 all worked, but in the latter case the maximum singular value approached unity in two places. With $n = 20$, both $m = 2$ and $m = 10$ made good designs. We comment that the inverse of a discrete time system transfer function with one time step delay from input to output (as one obtains from discretizing a differential equation fed by a zero order hold) is non-causal by one time step. And this corresponds to $m = 2$. If one uses a large value for m, then one is looking at a large number of time steps into the future of the present phase but during the previous period. The best values of m here do not do this.

The period of the periodic desired output is $p = 60$ time steps wit sample time interval $T = 1/8$ s, and this corresponds to 7.5 seconds. The control being picked at time step k is the control used one period back at $k - p$ plus a linear combination of the errors at time steps from $k - p + m - 1$ back to time step $k - p - (n - m)$. Before one can start up the repetitive

controller, one needs data for all of these time steps. For the case studied in this section, for one of the values of m one can start at time step 88 and for the other, one must wait for time step 89. We turn the RC system on at time step 89, and this is time 11.125 seconds.

Figure 4.2 shows poles and zeros of 1,1 component of the continuous time transfer function matrix $G(s)$, corresponding to the transfer function from input on the first mass to the resulting output of that mass. The plot is for $\zeta = 0.2$, or 20% of critical damping. There are of course, three vibration modes corresponding to the poles, and then there are two complex conjugate sets of zeros. The corresponding plot for the 2,2 component is very similar with the same poles, but the zeros with the real part near -3 have moved to real part near -2.6, and the other pair with real part near -0.8 have moved the real part near -1.2. Figure 4.3 shows the poles and zeros of the 1,2 component of $G(s)$, and we notice that there are two non-minimum phase zeros and a real zero on the negative real axis. The 2,1 component is the same.

We consider that the inputs to this transfer function matrix come through a zero order hold, and there is a z-transfer function equivalent matrix $G(z)$. What the multiple SISO approach uses for design is the inverse of this matrix $H(z) = [G(z)]^{-1}$. Figure 4.4 shows the poles and zeros of the 1,1 component, and Figure 4.5 shows the same for the 1,2 component. Performing the operations one notes that one often encounters analytical cancellation of poles and zeros in the resulting z-transfer function matrix. The poles and zeros shown are those obtained by Matlab without performing these cancellations. In Figure 4.4 there seems to be 7 pole-zero cancellations, leaving one with 4 zeros and 3 poles. The poles and zeros are inside the unit circle. For the 2,2 element the pole-zero pattern is similar but again the real parts of the zeros have changed. The pair with real part near 0.6 has moved this value to roughly 0.75, and the pair near real part -0.1 has moved it to about -0.25. The plot for the 2,1 component is the same as for the 1,2 component.
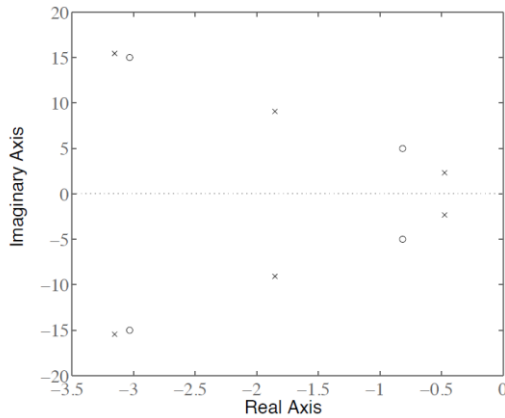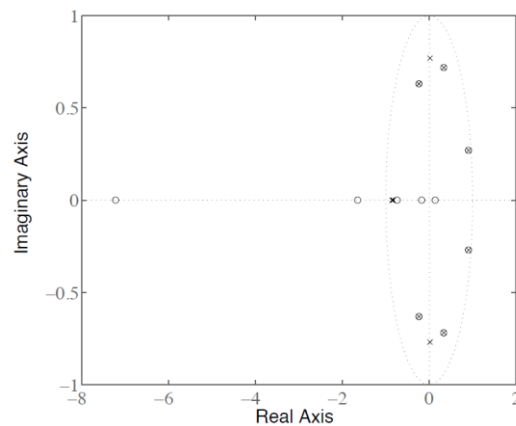
Figure 4.2 Poles and zeros of
$G_{11}(s)$ **for 20% damping**
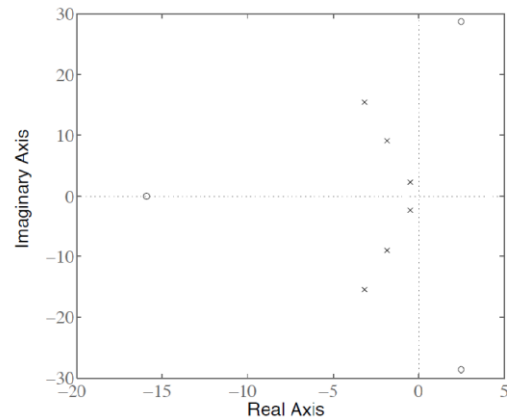
Figure 4.3 Poles and zeros of
$G_{12}(s)$ **for 20% damping**
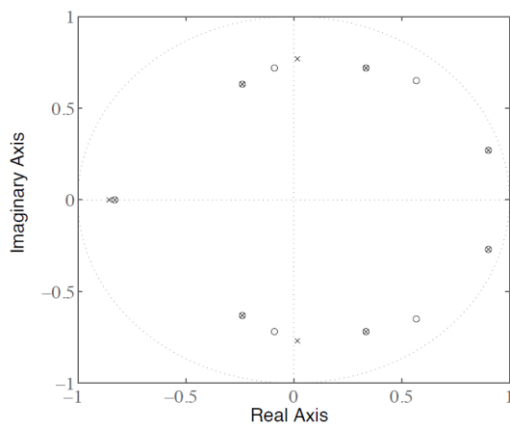
Figure 4.4. Poles and zeros of the 1,1
component of $G^{-1}(z)$ **for 20% damping**

Figure 4.5 Poles and zeros of the 1,2
**component of** $G^{-1}(z)$ **for 20% damping**

Note that what are used in the SISO designs are not these components, but their reciprocals. Hence, $\left[h_{ij}(z)\right]^{-1}$ used in the cost functions equation (4-3) have the zeros turned into poles, and the poles turned into zeros from Figures 4.4 and 4.5. Note that this creates a very non-standard SISO design problem for $[h_{12}(z)]^{-1}$ from Figure 4.5, because it has poles outside the unit circle. One expects that the optimization will approximately place zeros on top of these poles. And this possibility needs to be added to the procedure for setting n and m described

above for SISO problems. None of these examples here encounter zeros outside the unit circle during the design process.

The cost functions equation (4-3) aim to make $\left[h_{ij}(e^{i\omega T})\right]^{-1}\left[f_{ij}(e^{i\omega T})\right]$ as close to one as possible over all frequencies from zero to Nyquist. Figure 4.6 and 4.7 plot these complex numbers for the 1,1 component (the 2,2 component is very similar) and for the 1,2 component. These show that the RC design is making the frequency response of each component of $H(z)F(z)$ match the corresponding component of the identity matrix to within about 0.05 unit. Figure 4.8 plots the maximum singular value of the matrix $I - G\left(e^{i\omega T}\right)F(e^{i\omega T})$. With the maximum singular value being about 0.05 the system is guaranteed to be asymptotically stable. Figure 4.9 shows the error in each output and we observe that it has good performance. Figure 4.10 shows the root mean square of the error (RMS) for each period (repetition, or iteration) versus repetition, and we observe convergence to a numerical zero error in 20 repetitions.

Corresponding results were obtained for 10% damping and for 1% damping. Note that a system with 1% damping is not very stable, and its phase frequency response changes very fast with frequency going past a resonance, making it more difficult to capture the behavior of the inverse of the frequency response in an FIR filter. The plot corresponding to Figure 4.2 look identical to Figure 4.2 except that the horizontal axis that ends at -3.5 for 20% damping, ends at about -1.6 for 10% damping, and at -0.16 for 1% damping. Figure 4.3 changes in the following way: the poles must change their angle α made with the negative real axis to correspond to $\zeta = \cos\alpha$; the zeros for 20% damping roughly located at -16 and $2.5\pm19i$, move to -23 and $14\pm33i$ for 10%, and to -60 and $30\pm60i$ for 1%. Figure 4.4 looks similar for all three cases, except that all poles and zeros get much closer to the unit circle. The main change seen in Figure
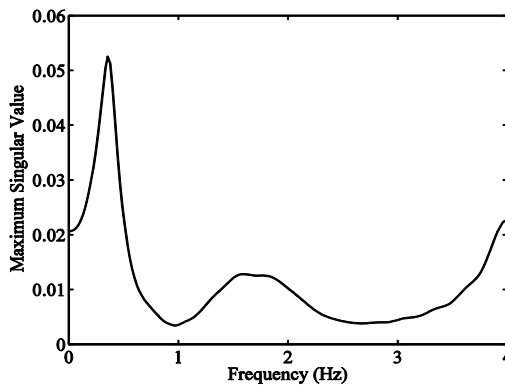
4.5 is that zero locations roughly at -1.5, -7.5 move to -2.5, -12.5, and then to -4, -32, going very
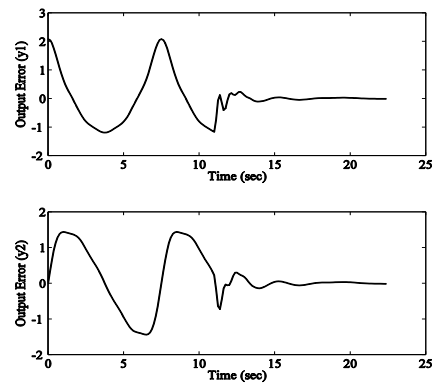
far outside the unit circle.
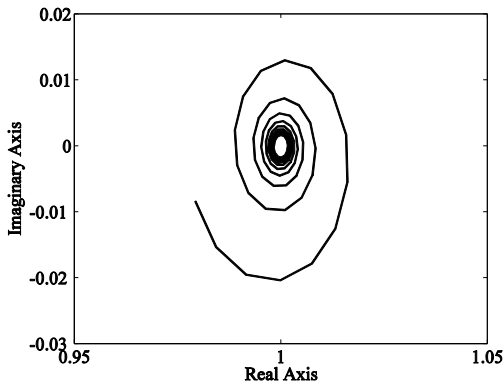
Figure 4.6 Plot of $[h_{11}(e^{i\omega T})]^{-1} f_{11}(e^{i\omega T})$ **from zero to Nyquist for 20% damping**
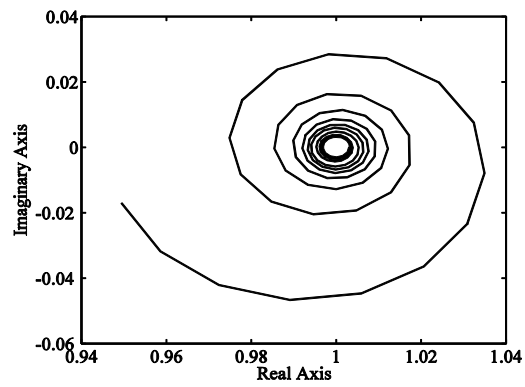
Figure 4.7 Plot of $[h_{12}(e^{i\omega T})]^{-1} f_{12}(e^{i\omega T})$ **from zero to Nyquist for 20% damping**

Figure 4.8 Plot of the maximum singular value of $I - [H(e^{i\omega T})]^{-1} F(e^{i\omega T})$ **from zero to Nyquist for 20% damping**

Figure 4.9 Plot of output error versus time, RC turned on at 11.125s, period is 7.5s, 20% damping

Figure 4.7 gives a range of error in matching unity over all frequencies, and the error is

the radial distance from +1 to any point on the plot corresponding to a certain frequency. The

real part of ranges from about 0.95 up to about 1.03, differing from +1 by only 5%. For 10%

damping this range is roughly from 0.68 to 1.13. Cost functions in equation (4-3) still did a good

job, producing asymptotic stability with the maximum singular value for each frequency given

by Figure 4.11. This still produces fast learning, heuristically estimated as having the error decay by a factor of 1/3 each period according to Reference [42].

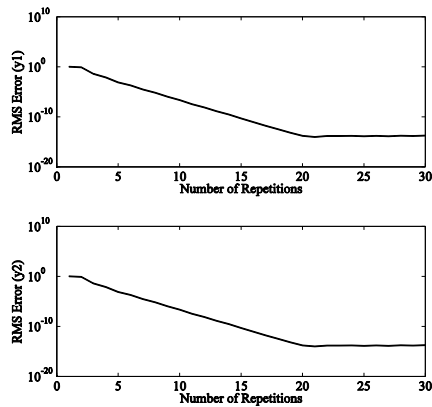**Figure 4.10 Plot of the RMS of the output error each iteration versus iteration number, 20% damping**

Figure 4.11 Plot of the maximum singular value of $[I - H(e^{i\omega T})]^{-1}F(e^{i\omega T})$ from zero to Nyquist for 10% damping
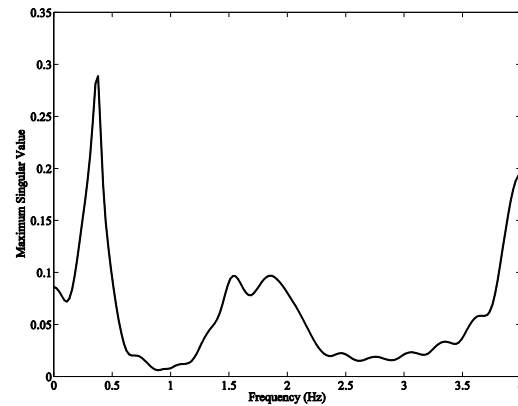
Figures 4.12, 4.13, and 4.14 give 1% damping plots corresponding to Figures 4.6 and 4.7. The FIR filters with $n = 30$ no longer giving a good approximation of the MIMO inverse frequency response. Figure 4.15 shows the corresponding singular value plot for sufficient stability condition equation (3-32). To obtain an effective design, one might consider using $n = 60$ as is done in the next section with asymptotically stable results. Because a very lightly damped resonant peak has very fast phase change in a short frequency range, one might also modify the number and distribution of the discrete frequencies used in the cost functional summations. And of course one could consider using the weighting factor W_k to force a better fit in the region of importance. Note that each cost function individually keeps the RC design within what would be the stability boundary for real SISO systems, but the combination of the SISO designs does not have the same monotonic decay property for MIMO. This points out the difference between aiming to minimize the equation errors in $I - H(z)F(z)$ and aiming to satisfy the sufficient stability condition equation (3-22).
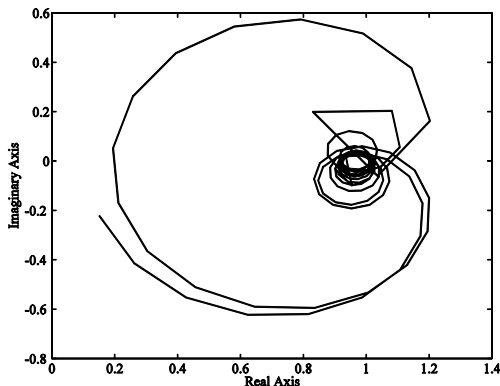
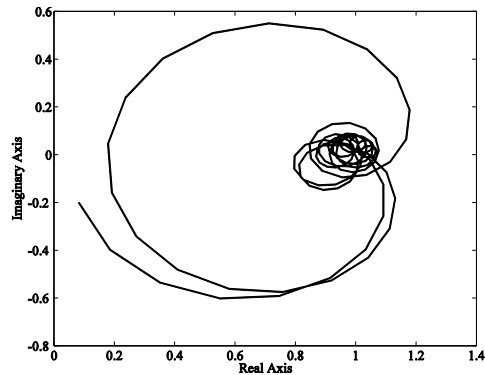**Figure 4.12 Plot of $[h_{11}(e^{i\omega T})]^{-1}f_{11}(e^{i\omega T})$ from zero to Nyquist for 1% damping**

Figure 4.13 Plot of $[h_{22}(e^{i\omega T})]^{-1}f_{22}(e^{i\omega T})$ from zero to Nyquist for 1% damping
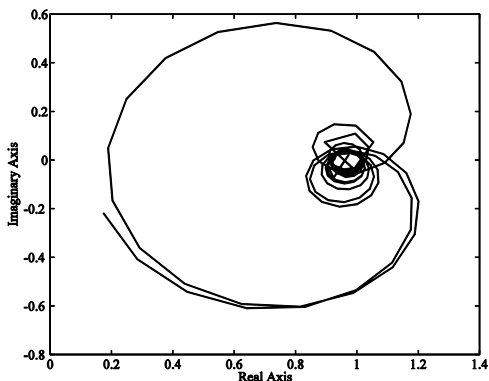
Figure 4.14 Plot of $[h_{12}(e^{i\omega T})]^{-1}f_{12}(e^{i\omega T})$ or of $[h_{21}(e^{i\omega T})]^{-1}f_{21}(e^{i\omega T})$ from zero to Nyquist for 1% damping
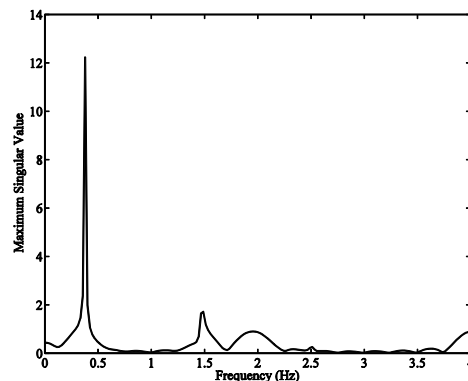
Figure 4.15 Plot the maximum singular value of $I - [H(e^{i\omega T})]^{-1}F(e^{i\omega T})$ from zero to Nyquist for 1% damping

4.5 Numerical Results Designing RC Using the Frobenius Norm Cost Functional

When designing a MIMO RC system using the cost functional equation (4-4) one specifies the choice of n that specifies the number of gain matrices, and m specifies the range of these gain matrices associated with the tracking error from time step $k - p + m - 1$ to time step $k - n + m - p$, when k is the current time step. In this design approach the same choice applies to all input-output pairs in $G(z)$. In the following simulation, the period of the desired trajectory is 60 time steps, hence $p = 60$. First, we consider the simplest design possible with just 2 gain

matrices, $n = 2$. We also choose the best value of m which comes very close to satisfying sufficient stability condition equation (3-32), which is $m = 2$. The repetitive controller in this case has the form $u(k) = u(k - 60) + a_1 e(k - 59) + a_2 e(k - 60)$. Each a_1 or a_2 is a 2-by-2 matrix. Figure 4.16 shows these gain values. The diagonal gains correspond to the first-input-to-first-output, and the second-input-to-second-output pairs. The off-diagonal gains correspond to the first-input-to-second-output, and second-input-to-first-output pairs. Equation (3-32) is a condition for quasi-steady-state monotonic convergence of the norm of the tracking error from period to period, and it is a sufficient condition guaranteeing convergence to zero error. A plot of the left hand side of equation (3-32), i.e. the maximum singular value versus ωT from zero to Nyquist at $\omega T = \pi$ is shown in Figure 4.17. Except for a small frequency range this maximum singular value is less than one, suggesting that monotonic convergence is expected. The result of this test does not guarantee convergence to zero tracking error, but the tracking error from period to period is shown in Figure 4.18 and is seen to converge monotonically. Finally, Figure 4.19 shows the zeros of the controller transfer functions. Because this is a two-input two-output system, there are four such controller transfer functions. Each controller transfer function has p poles at the origin.

Next, we consider the case where we use a total of $n = p = 60$ gains while keeping $m = 2$. Figure 4.20 reveals that although 60 gain matrices are allowed, the optimization produces about 30-40 gains that are "significant", the magnitudes of the remaining gains are relatively small in comparison. Each plot contains two curves, but they are indistinguishable to plot accuracy. The maximum singular value is well below one as shown in Figure 4.21, suggesting monotonic convergence of all frequencies from period to period, and guaranteeing asymptotic stability and convergence to zero tracking error. Based on the speed of decay of the

error, the design is close to inverting the dynamic system. The rapid convergence of tracking error is indeed observed in Figure 4.22. There are now a large number of controller zeros, and they are all "stable" as shown in Figure 4.23, i.e. inside the unit circle.

Finally, we consider the case where $n = p = 60$, but m is increased to 30. Our preliminary observation suggest that there is no obvious benefit with using a large value for m. There are no significant changes in the controller gain magnitudes (Figure 4.24). The controller still approximates an inverse of the dynamic model (Figure 4.25). The convergence of the tracking error is therefore rapid (Figure 4.26). This time, however, we observe that there are a large number of "unstable" zeros associated with these controller transfer functions as shown in Figure 4.27. We observe that unlike the case of designing a repetitive controller for a single-input single-output system with a relatively small number of gains, the choice of the value of m appears to not be at all critical in these MIMO designs when n is large. We can understand this in terms of the following observation. If n is large enough that the gains taper off to essentially zero, then any change needed in the value of m is accomplished by just shifting all the gains one or more time steps in the needed direction. This is illustrated by comparing Figure 4.20 using $n = 60$ with $m = 2$, to Figure 4.24 with $n = 60$ with $m = 30$. The plots of the gains in each case look the same, but have been shifted an appropriate number of time steps to account for the different value of m used. The fact that there can be more nonzero but small gains in the $m = 2$ case allows the singular value plot to be better for this case (Figures 4.21 and 4.25), but the performance of the decay with repetitions does not seem to be affected (Figures 4.22 and 4.26). These observations suggest that the ability to individually adjust m for each entry in matrix $F(z)$ or the multiple SISO approach is only an important advantage if one keeps the value of n sufficiently small that the gains do not taper off to near zero.
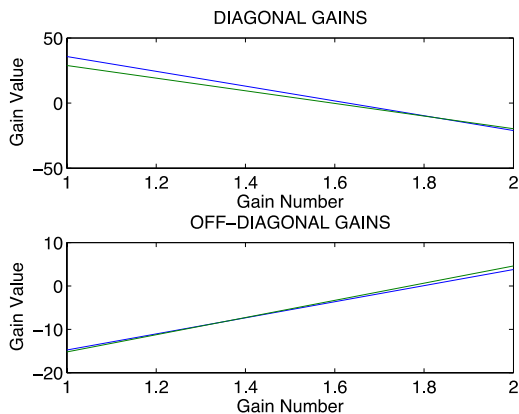
Figure 4.16 Repetitive control gains
($n = 2, m = 2$)
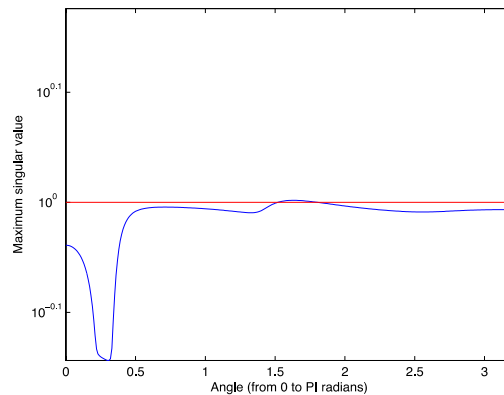
Figure 4.17 Maximum singular values
($n = 2, m = 2$)
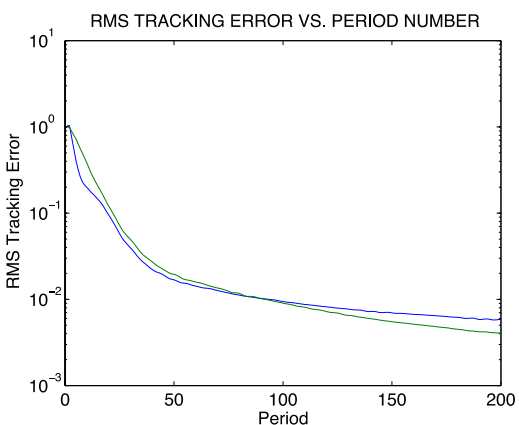
Figure 4.18 Convergence of RMS tracking
error ($n = 2, m = 2$)

Figure 4.19 Controller TF zeros
($n = 2, m = 2$)

Figure 4.20 Repetitive control gains
($n = 60, m = 2$)

Figure 4.21 Maximum singular values
($n = 60, m = 2$)

Figure 4.22 Convergence of RMS tracking error ($n = 60, m = 2$)

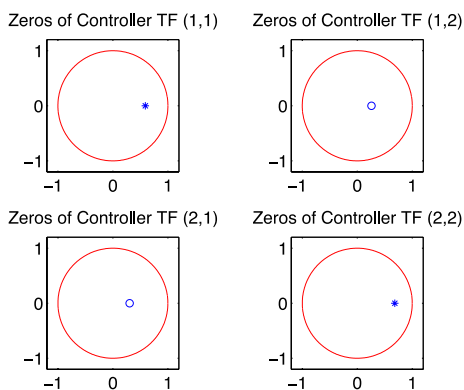**Figure 4.23 Controller TF zeros ($n = 60, m = 2$)**

F**igure 4.24 Repetitive control gains ($n = 60, m = 30$)**
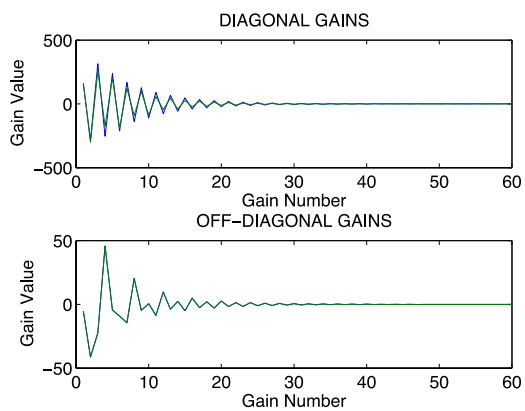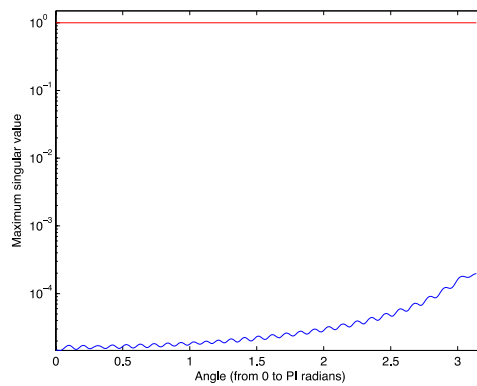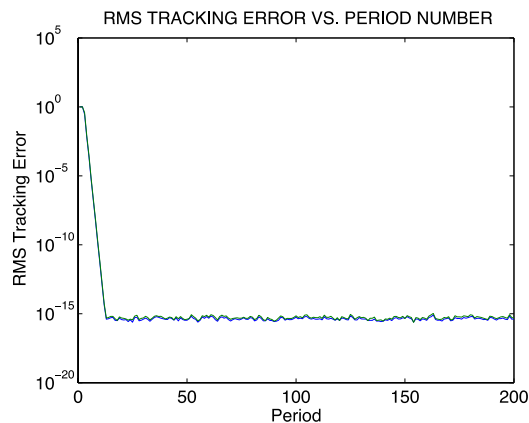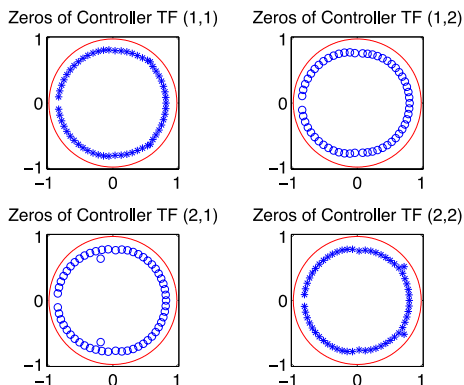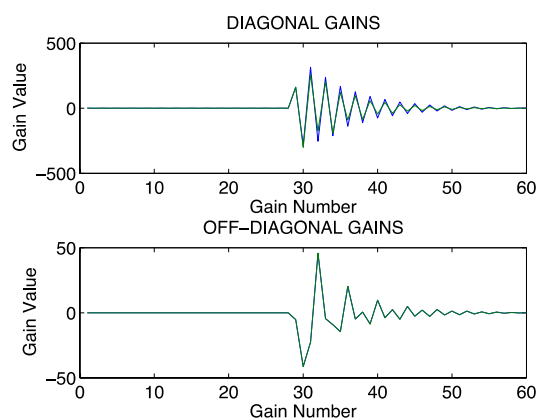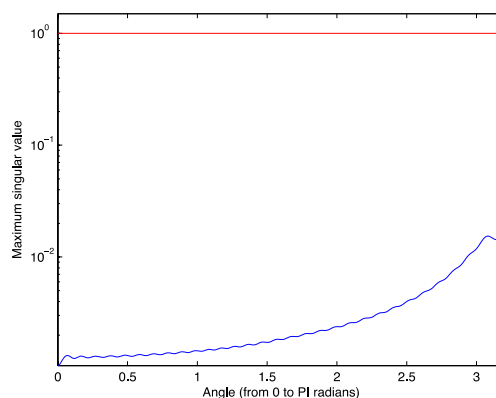

Figure 4.25 Maximum singular values ($n = 60, m = 30$)
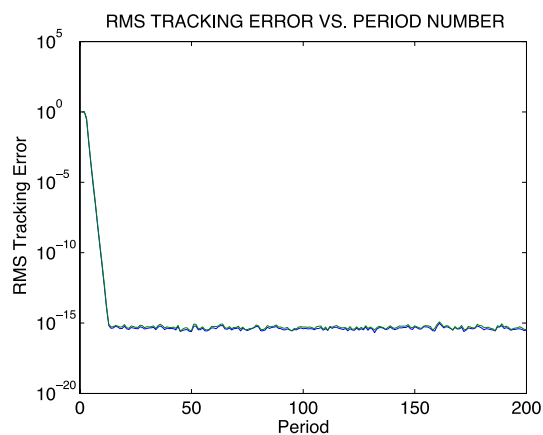
Figure 4.26 Convergence of RMS tracking error ($n = 60, m = 30$)
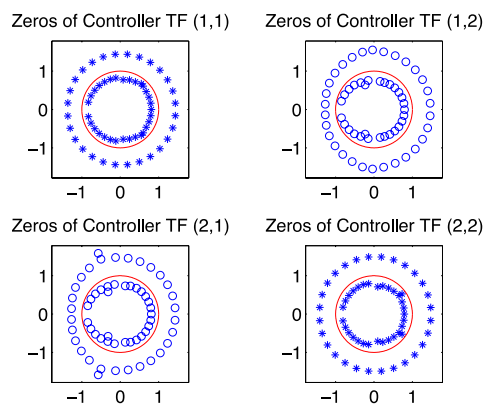
Figure 4.27 Controller TF zeros ($n = 60, m = 30$)

Chapter 5. Designing Learning Control that Is Close to Instability for Improved

Parameter Identification

5.1 A Condition for Decay or Growth of Error with ILC Iterations

This section presents the basic formulation and certain important properties of ILC. See reference [8] for more detail using the same approach. Let $y*(k)$ be a chosen desired system output that is p time steps long. In the first run or iteration, one applies a chosen p step input and records the response. After each iteration the system is reset to the same initial starting conditions, and the input is updated according to an ILC law and applied to the system. The usual objective of ILC is to obtain zero tracking error for every time step of this desired trajectory that is p time steps long. Thus ILC is asking for zero error during initial transients at the start of each run, not just in steady state as in RC. Also, there may be a disturbance function that appears every time one runs the trajectory, and the ILC should eliminate error from this source as well as the usual tracking error of a feedback control system.

Let subscript j denote the run number or iteration number, and write the real world dynamics as a single input, single output difference equation

$$x_j(k+1) = Ax_j(k) + Bu_j(k) \; ; \; y_j(k) = Cx_j(k) \tag{5-1}$$

Define the output error as $e_j(k) = y*(k) - y_j(k)$. The actual dynamics may be governed by a linear differential equation, and the input is applied through a zero order hold, holding $u_j(k)$ constant throughout time step k. Then (5-1) can represent this differential equation without approximation, and the original differential equation can be recovered uniquely provided the sample rate is high enough to avoid aliasing. Use underbars to indicate a column vector of the history of a variable for iteration j. Then $\underline{u}_j$ is a column vector of inputs $u(k)$ for time steps 0

through p - 1, and $\underline{y}_j$, $\underline{e}_j$ are similar except that they start and end one time step later. This one

time step shift is incorporated into the definitions to account for the usual one time step delay

between a change in the input and the first time step a change is seen in the sampled output. A

general linear ILC law takes the form $\underline{u}_{j+1} = \underline{u}_j + L\underline{e}_j$ where L is a p by p matrix of learning

control gains. One can write the solution to (5-1) for p time steps in terms of the convolution sum,

making use of the lower triangular Toeplitz matrix P of Markov parameters, whose diagonal

elements are all CB, all elements in the first subdiagonal are CAB, and continuing in this manner

to the element $CA^{p-1}B$ in the lower left corner. Then one can give the error history evolution

with iterations as

$$\underline{e}_{j+1} = (I - PL)\underline{e}_j \quad ; \quad \max_i \left| \lambda_i (I - PL) \right| < 1 \tag{5-2}$$

where I is the p by p identity matrix, and the second equation in (5-2) gives the stability

boundary, i.e. satisfying it guarantees convergence to zero tracking error for all possible initial

inputs.

Suppose that the matrix learning law L has a Toeplitz structure so that all entries along

any given diagonal are the same. Then L is a finite time version of a transfer function which we

denote as $L(z)$. Let $G(z)$ be the z-transfer function of system (5-1). Then one can take

transforms of the system and the learning law to obtain

$$E_{j+1}(z) = [1 - G(z)L(z)]E_j(z) \tag{5-3}$$

The square brackets represent a transfer function from the error in one iteration to that in the next.

Set $z = \exp(i\omega T)$ in this expression to form the frequency transfer function, where T is the

sample time and ω is the radian frequency. If inequality

$$\left| I - G(e^{i\omega T})L(e^{i\omega T}) \right| < 1 \quad \forall \omega \tag{5-4}$$

is satisfied for all frequencies, then every steady state frequency component of the error will decay monotonically with iterations. This does not guarantee stability because of the transient parts of the trajectory. But if one makes p large enough compared to the time constants of the system and picks an appropriate $\underline{y}*$, the behavior described by (5-4) will dominate the responses for the early iterations, even if the learning process is actually unstable [35]. We will often study the learning behavior of (5-4) by plotting $G(z)L(z)$ for $z = \exp(i\omega T)$ for ωT from zero to π, i.e. from zero frequency to Nyquist frequency.
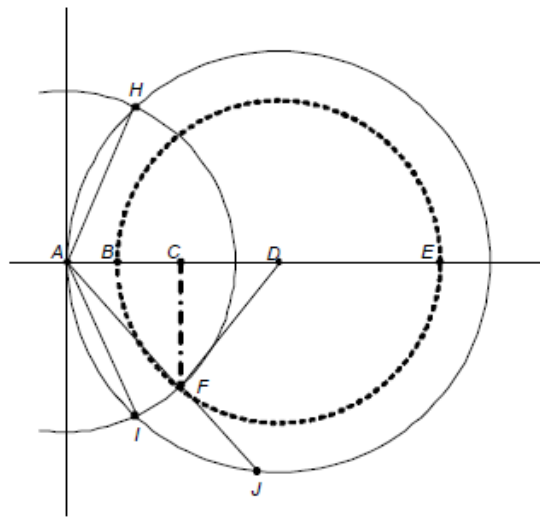
Figure 5.1 Definitions of circles and points for polar plots of frequency response of learning law times system

When plotted as in Figure 5.1, if the curve stays inside the unit circle centered at +1, (5-4) is satisfied at all frequencies. The radial distance from +1 to a point on the curve for a specific frequency indicates the factor by which the amplitude of a component of the error at that frequency will be multiplied every iteration. If that number is greater than one, that frequency component is amplified every iteration. The design problem for ILC requires producing a compensator that moves the curve inside the unit circle for all frequencies in order to produce

decaying error. Our objective is to make an ILC law that is deliberately non robust, so that small errors in the parameters of the model used for the ILC design will make the ILC iterations become unstable. We will do this by designing a learning law that moves all frequencies to points that are inside the unit circle based on the current model. But the points are chosen to be very near the stability boundary so that small model errors are likely to put the learning process outside the unit circle. Then the error components for those frequencies for which the model was inaccurate enough to make the ILC unstable, will grow with iterations. With enough iterations the errors will be arbitrarily amplified so that system identification will be able to see and correct the parameter error.

5.2 Creating a Deliberately Non Robust ILC Law

Reference [34] develops a phase cancellation ILC law. The error is decomposed into its frequency components, a phase lead (or lag) is introduced in each component such that when it goes through the system, the system supplies the opposite phase lag (or lead). In this way every component of the error after going through the ILC law and then the system will be real and positive. This means that the plot of $G(z)L(z)$ for $z = \exp(i\omega T)$ is on the positive real axis in Figure 5.1. And an appropriately chosen gain will keep it smaller than 2 so that (5-4) is satisfied. Experiments in [34] on a robot performing a high speed maneuver decreased the root mean square of the tracking error by a factor of nearly 1000 in about 15 to 20 iterations. Note that numerical studies suggest that this learning law is actually unstable, i.e. it does not satisfy inequality (5-2). Simulations will be documented elsewhere that show small wiggles near the end of the trajectory start to become evident by iteration 1000. The onset of these wiggles can be delayed by including a constant section of trajectory at the end. In any case the instability takes many iterations to appear, and it appears starting from the end of the trajectory, while lack of

satisfying (5-4) creates growth of error for all time steps after a settling time of the system, i.e. once steady state frequency response thinking applies. These different signatures make the two sources of growth easily distinguishable if the trajectory is chosen substantially longer than one settling time of the system.

It is this phase cancellation law that we seek to alter: instead of placing the plot of $G(z)L(z)$ on the positive real axis, we seek to place it on a circle of chosen radius r_1 (length DF in Figure 5.1) which is inside the unit circle. This is done using our current model which we denote by $G_n(z)$ (with corresponding magnitude $r_n(\omega)$ and phase angle $\theta_n(\omega)$ made with the positive real axis, for $z = \exp(i\omega T)$) creating the learning law $L_n(z)$. When we study how it behaves when applied to a real world that is different than our current model, we denote the real world behavior by $G_r(z)$ (with corresponding r_r, θ_r). Since circle r_1 is inside the unit circle, inequality (5-4) is satisfied for the nominal model, but if radius r_1 is near unity, then one expects that small model errors will send the learning process unstable. A question to be addressed is, how do we choose what frequency between zero and Nyquist should be placed at each point on this circle. Two methods will be suggested and studied.

The most common source of instability in ILC comes from phase inaccuracy of the model at high frequency, often due to missing high frequency dynamics. A missing high frequency pole introduces more phase lag at high frequency than in the nominal model. This suggests that one place all frequencies on the lower half of the circle. Here we are interested in parameter errors, and one expects that parameter errors of one sign will produce a positive phase error, and of the opposite sign will produce a negative phase error. For this reason, we investigate using two ILC iterations, one mapping points to the lower half of the circle, and the other mapping to the upper half. The degree to which this is effective will be investigated.

The learning law is developed as follows. Given the p time step history of the error, one can see approximately $p/2$ discrete frequencies. These frequencies are related to $(2\pi / pT)j$ for $j = 0,1,2,..., p-1$, corresponding to these numbers up through Nyquist frequency and then folding onto existing frequencies below Nyquist. Define $z_0 = \exp(i2\pi / p)$ and construct matrix H whose α, β component is given by $H_{\alpha\beta} = z_0^{-(\alpha-1)(\beta-1)}$. Then $H\underline{e}$ produces the discrete Fourier transform (DFT) of the error vector, where the first element is related to DC, the next element and the last element combine to form the frequency component related to discrete frequency $2\pi /(pT)$, etc. In the frequency domain, our objective is to create $L_n(z)$ to satisfy

$$L_n(e^{i\omega T})G_n(e^{i\omega T}) = r_2(\omega)e^{i\theta_2(\omega)} \quad ; \quad L_n(e^{i\omega T}) = [r_2(\omega)/r_n(\omega)]e^{i(\theta_2(\omega)-\theta_n(\omega))} \tag{5-5}$$

Here, the chosen location for frequency ω is point F in Figure 5.1 with AF being of length $r_2(\omega)$, and the angle DAF being $\theta_2(\omega)$ except that we wish to measure this angle in a manner consistent with the associated phase lag and hence make it measured positive in the counterclockwise direction (the angle is negative for the point F as pictured). In matrix form we can produce this change in magnitude and phase for each of the elements related to its discrete frequency, by pre-multiplying $H\underline{e}$ by a diagonal matrix given by

$$\Lambda = diag\left[\left(\frac{r_2(\omega_j)}{r_n(\omega_j)}\right)e^{i[\theta_2(\omega_j)-\theta_2(\omega_j)]}; \omega_j = \frac{2\pi}{pT}j; j = 0,1,2..., p-1\right] \tag{5-6}$$

Note that $j=1$ and $j=-1$ that are associated with the same frequency, have opposite signs in the exponential. And the frequencies in (5-6) go up to two Nyquist, doing so in such a way as to accomplish the desired phase change with the right sign in both terms. Then one must convert back to the time domain using $H^{-1} = (1/p)(H*)^T$ where the asterisk denotes the complex conjugate, and T is the transpose. The resulting learning law is

$$\underline{u}_{j+1} = \underline{u}_j + L_n \underline{e}_j = \underline{u}_j + (1/p)(H^*)^T \Lambda H \underline{e}_j \qquad (5\text{-}7)$$

5.2.1 Mapping Linearly with Central Angle

One choice for the mapping onto the circle of radius r_1 is to map these points linearly with frequency to the angle θ_1 corresponding to $\angle EDF$, measured positive clockwise for placement on the lower half of the circle and positive counterclockwise on the upper half, starting at zero frequency at angle zero, and ending at Nyquist at angle 180°. This produces $\theta_1(\omega) = \omega T$. In order to use this statement to produce the control law (5-7) we need to compute for each frequency what the polar coordinates r_2, θ_2 are for the chosen point F. We will need the law of cosines for general triangles which says that the square of the length of one side is equal to the sum of the squares of the other two sides minus two times the product of these two sides times the cosine of the angle between them. Use triangle ADF to compute r_2 which is AF, and AD is one, DF is r_1, and $\angle ADF$ is $\pi - \theta_1$. To find θ_2 which is $\angle DAF$ (but adjusted for the sign convention), again use triangle DAF, but this time adjust the choice of sides in the law of cosines so that the angle involved is $\angle DAF$, and then solve for this angle. The results are

$$r_2 = sqrt[1 + r_1^2 - 2r_1 \cos(\pi - \theta_1)] \; ; \; \theta_2 = \pm a\cos[(1 - r_1^2 + r_2^2)/(2r_2)] \qquad (5\text{-}8)$$

The negative sign is used for mapping to the bottom half of the circle, and the plus used for mapping to the top half.

5.2.2 Mapping Linearly with Horizontal Component

Consider a second choice that maps frequencies onto the chosen circle starting with zero frequency at point E, and progressing to Nyquist at point B, and doing so with the frequency made linear in the horizontal component x of point F, i.e. $x = 1 + r_1$ corresponds to $\omega T = 0$ and

$x = 1 - r_1$ corresponds to $\omega T = \pi$. Given this x which is the horizontal component of point F, we can compute the vertical component y, by using $(x-1)^2 + y^2 = r_1^2$, picking y as negative for mapping to the bottom half, and positive for the top half. Then the needed polar coordinates are $r_2 = sqrt(x^2 + y^2)$ and $\theta_2 = atan2(y, x)$, where the arc tangent function of two arguments is used in order to have the right quadrant for the result.

5.2.3 Computing Stability Limits on Phase and Gain Error

Consider that we have designed $L_n(z)$ based on our current system model $G_n(z)$ according to equation (5-5) (and in matrix form (5-6, 5-7)), and we apply it to the real world hardware whose transfer function is $G_r(z)$. The intended point for frequency ω is point F given by $r_2(\omega)\exp[i\theta_2(\omega)]$. The actual point produced is given by

$$L_n(e^{i\omega T})G_r(e^{i\omega T}) = L_n G_n\left(\frac{G_r}{G_n}\right) = r_2(\omega)e^{i\theta_2(\omega)}\left(\frac{r_r(\omega)}{r_n(\omega)}\right)e^{i(\theta_r(\omega)-\theta_n(\omega))} \tag{5-9}$$

It is of interest to determine what the limits are on the phase angle error $\theta_r - \theta_n$ before inequality (5-4) is violating and the iteration makes certain frequency components of the error grow. Similarly we are interested in the maximum value of r_r / r_n before magnitude error produces growth. Two limits on phase error for point F are an additional phase lag corresponding to $\angle FAI$ and a phase lead corresponding to $\angle HAF$. Of course, if we are interested in the limits when mapping to the upper half of the circle, the same limits will apply but with reversed sign, so we only consider mapping to the lower half. We need to find $\angle DAI$, and then knowing $\angle DAF$ from the θ_2 computation above, allows one to sum the angles for the positive tolerance $\angle FAH$ and difference them for the negative tolerance $\angle FAI$.

First we find the horizontal component x_I of point I (or H), by noting that this point is on two circles: $x_I^2 + y_I^2 = r_2^2$ and $(x_I - 1)^2 + y_I^2 = 1$. Substituting the left hand side of the first into the second produces $x_I = r_2^2/2$, and substituting this into the first produces $y_I = -r_2 sqrt(1 - r_2^2/4)$. Then $\angle DAI$ is given by the arc tangent of y_I/x_I. Figure 5.2 plots the results. The solid lines are the upper and lower limits for phase error using $r_1 = 0.95$, and the dashed lines are for $r_1 = 0.9$. The top left plot uses linear in central angle, and the top right uses linear in horizontal component. Figure 5.3 gives a detailed view. This time the solid lines are for linear in horizontal component with the upper plot of the two being for radius 0.95. The dashed lines are corresponding curves for 0.90. We see that linear in horizontal component is much more uniform in its sensitivity to phase lag, and hence is to be preferred. Both approaches have a minimum tolerance of -2.865° for radius 0.95, and of 5.732° for radius 0.90. One would expect that such a tight robustness limit would make ILC very effective at producing data that is amplified where the model is wrong even by a small amount. Figure 5.3 shows the detail of stability limit on phase error using linear in horizontal component law.

To study the magnitude tolerance, we need to find point J. Triangle DAJ is an isosceles triangle and we know $\angle DAJ$. Bisecting $\angle ADJ$ forms a right triangle whose base is half the maximum r_r allowed, and whose hypotenuse is unity. Hence, $r_r = 2\cos\theta_2$. The bottom left plot in Figure 5.2 gives r_r/r_n versus percent Nyquist frequency for linear in central angle, and the bottom right plot gives the corresponding plot for linear in horizontal component. Note the only possibility for going unstable is an increase in the amplitude of the output.
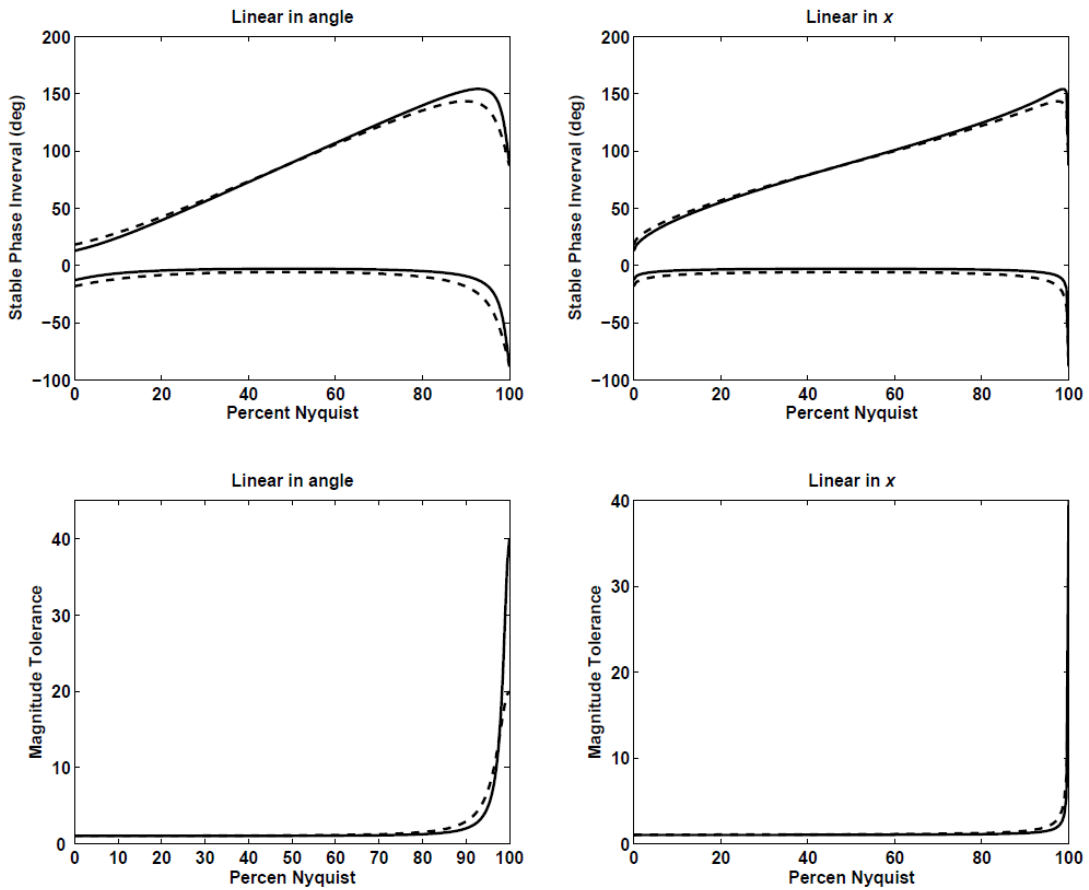
Figure 5.2 Stability limits on phase error (top) and magnitude error (bottom) for linear in central angle (left) and linear in horizontal component (right)
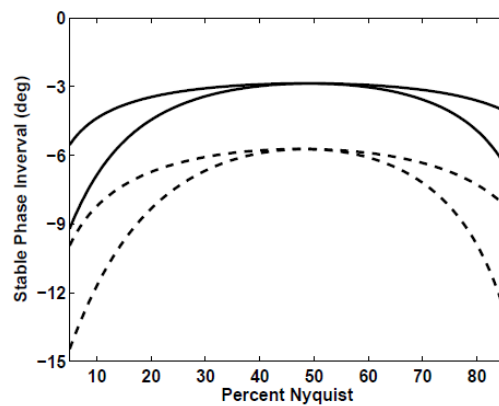
Figure 5.3 Detail of stability limit on phase error using linear in horizontal component law

5.3 Numerical Investigation of Sensitivity to Parameter Error

A simple but rather good model of the input to output transfer function for the feedback control systems for each link of the robot used in experiments in [34] is given in Laplace transfer function form as

$$G(s) = \frac{K}{(s+a)(s^2 + 2\zeta\Omega s + \Omega^2)} \tag{5-10}$$

where $a = 8.8$, $\zeta = 0.5$, $\Omega = 37$, and $K = 8.8*(37)^2$. We choose to discretize this as fed by a zero order hold sampling every $T=0.01$ seconds, and then regard the resulting transfer function as the current model $G_n(z)$. Consider the linear in horizontal component ILC law above with $r_1 = 0.95$. Then Figure 5.4 plots equation (5-9), applying this learning law to real world models $G_r(z)$ that corresponds to having the parameters a, ζ, Ω individually changed by +10% and by -10%. The lower half of each plot corresponds to mapping onto the lower half of the circle of radius r_1, and the upper half of the figures gives the corresponding results for mapping onto the upper half of the circle. Any frequency component that plots outside the unit circle centered at +1 will grow with iterations by an amplification factor equal to the radial distance to that point on the curve. Letting it grow for enough iterations, will make arbitrarily large this part of the system response that is not properly predicted by the nominal model. Hence, it can pull the errors out of the noise level and produce data that is rich in information about the model error. For the case of the actual frequency Ω being 10% smaller than in the current model, i.e. the lower right plot in Figure 5.4, the curve reaches a radial distance from +1 of 1.47 at frequency 3.5 Hz and hence will grow large within a few iterations.

The original objective of doing one iteration with the ILC mapping to the lower half of the circle and one ILC mapping to the upper half of the circle, was to have one of the two be sent

unstable when there is a relatively small phase error. Examining Figure 5.4 we see that when a or ζ is increased by 10%, both mappings send the plot in the stable direction so that neither one produces data that helps identify errors in this direction for these parameters. In the case of increasing Ω, using both mappings has the intended effect: when using the upper mapping the ILC becomes unstable while it stays stable with the lower mapping. When the parameters are decreased by 10% all cases result in instability whether mapping to the lower half or the upper half.

The behavior for parameter a can be understood by considering that it is not only the phase that changes, but also the magnitude. When a is increased, the phase angle is less than expected at all frequencies which should send the plot in the stable direction when mapping to the lower half, and toward the unstable direction when mapping to the upper half. However, when a is increased by 10% for the real world compared to the model, the learning law has placed the DC gain smaller than anticipated, which pulls both plots in the stable direction. The same effect is happening at other frequencies as well. Based on the top left plot in Figure 5.4, it appears that the second effect overpowers the first and prevents the mapping to the upper half from producing instability.
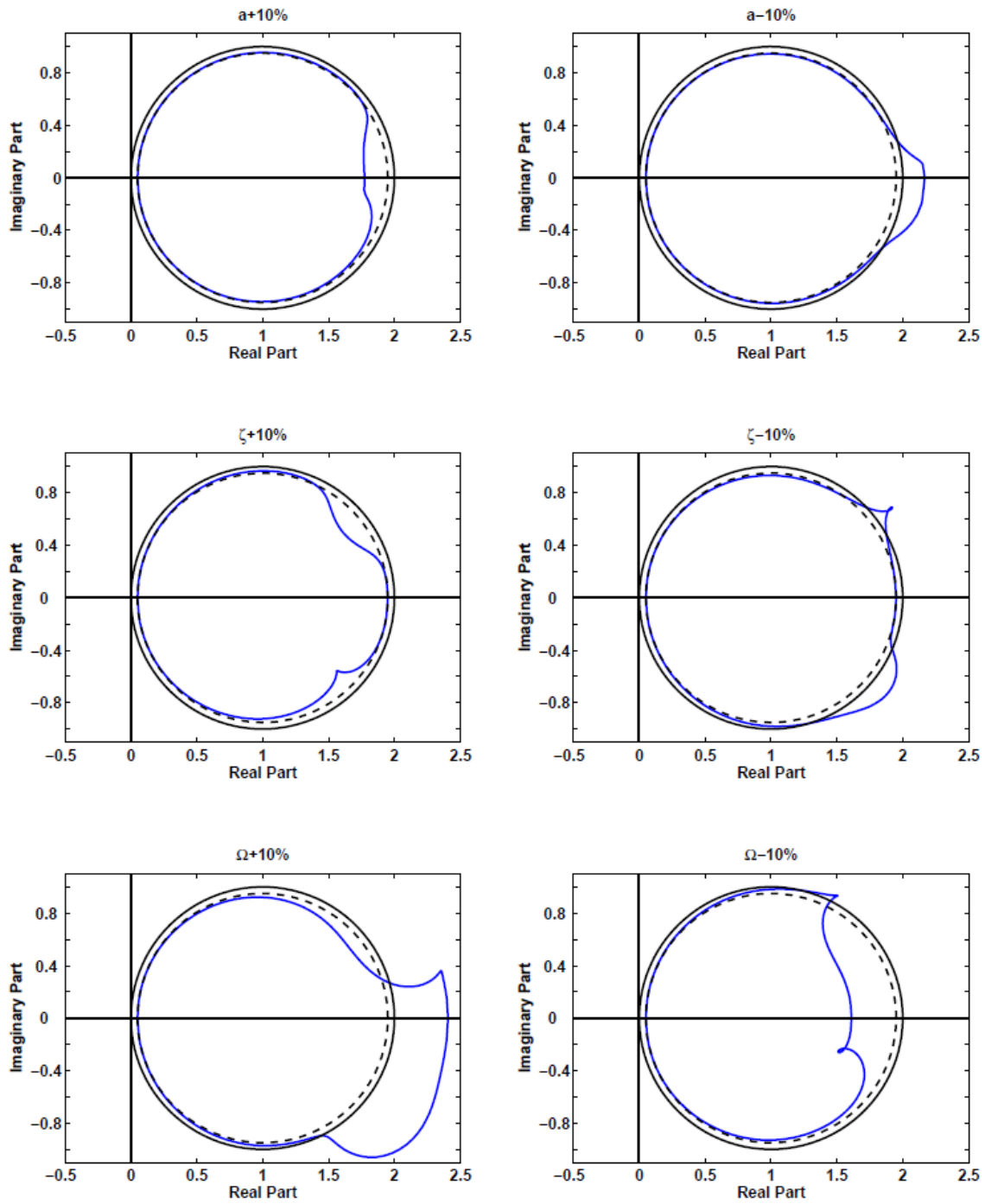
Figure 5.4 Polar plots with *a*, *ς*, Ω changed

Chapter 6. Conclusions

6.1 Taylor Series Expansion RC Design

Chapter 2 presents a new method to design repetitive controllers based on creating a non-causal FIR filter that approximates the frequency response of the system inverse using Taylor series expansions. Repetitive control would like to use the inverse of the system transfer function as a compensator, but since discrete time systems usually have zeros outside the unit circle this inverse in unstable. Here the inverse of a zero outside, i.e. a pole outside, is mimicked by a Taylor series using a chosen number of terms, which can also be thought of as introducing a new set of zeros. The approximate inverse can be good in terms of approximating the frequency response of the system, and a sufficiently good approximation of the inverse of the frequency response of the system is sufficient to produce stability. The approach is simple and gives considerable insight. Methods are developed to help pick the order of the compensator in order to reach desired error levels in the approximation of the inverse system frequency response. It is also shown how the insight gained by this approach can guide the choice of parameter values when using the repetitive controller design method that optimizes the compensator based on frequency response.

6.2 Stability of MIMO Repetitive Control Systems

In Chapter 3, the MIMO equivalent of the heuristic monotonic decay condition was generated, and developed the necessary and sufficient condition for asymptotic stability of the MIMO repetitive control system was developed. We also proved that the MIMO heuristic monotonic decay condition is a sufficient condition for asymptotic stability and hence convergence to zero error. This result started from first principles, and made use of an approach

similar to the Nyquist stability criterion. But the approach succeeds in avoiding the need to use a contour that goes around each of the p poles on the unit circle in the open loop transfer function, something that makes direct application of Nyquist condition intractable in many problems. This result is stated in Theorem 1.

Another stability condition is derived that is also a necessary and sufficient stability condition, but for repetitive control systems that are required to be asymptotically stable for all possible specified periods p of the periodic command or periodic disturbance. This result is presented in Theorem 2.

Next, a set of four sufficient conditions for asymptotic stability of repetitive control systems is generated. This includes the expected condition on the maximum singular value of the repetition update, but includes two conditions that are closer to the necessary and sufficient stability boundary. Each can be used to test the stability of a candidate design. These are summarized in Theorem 3.

The MIMO design is generalized to allow use of an FIR zero-phase low-pass filter to robustify the repetitive control process to parasitic poles or unmodeled high frequency dynamics, making use of the filter design process in [14,15]. This is stated in Theorem 4.

6.3 MIMO RC Design Methods

Based on the theoretical stability conditions of Chapter 3, Chapter 4 creates two MIMO RC design methods. One method is to design MIMO repetitive control systems using separate SISO repetitive control system designs for each component. One can apply this approach using a MIMO system model, or one can directly use input-output data to create frequency response information, without needing a model. Another method uses an optimization criterion based on a Frobenius norm to design RC controllers for MIMO systems based on optimization in the

frequency domain. This criterion has an analytical formula for the optimal design. The criterion is the MIMO analog of the FIR compensator design method in [7], also discussed in section 4.2. This method can also be applied directly to experimental frequency response data without needing to obtain an analytical model.

Chapter 4 studies and compares these two competing methods. It is seen that each approach can be effective. And each approach aims to minimize the equation error in $I - G(e^{i\omega T})F(e^{i\omega T}) = 0$ for all frequencies, but they aim to do so in different ways. One design aims to minimize the square of the Frobenius norm of the left hand side of this equation summed over frequencies from zero to Nyquist. This is the MIMO generalization of the SISO design method of Reference [7], but it is shown that in the latter case the approach is directly addressing the stability boundary, whereas in the MIMO case what it aims to minimize is a sufficient condition somewhat removed from the actual stability boundary. The approach based on making a set of SISO designs tries to make a design in which each component of the compensator looks as much as possible like the corresponding component of the inverse of the system transfer function, for all frequencies between zero and Nyquist. And this indirectly minimizes the equation error. There is considerable understanding and insight in picking the values of n and m in the FIR filters in $F(z)$ when done separately as in this SISO approach, and the approach allows one to use different values for each of the transfer functions of the input-output pairs. This intuition is lost when using the Frobenius norm cost functional, and the same choices for n and m apply to all input-output pairs, but numerical experience suggests that the selection of m is not critical at least for reasonably large values of n, the size of the FIR filter. Hence, what appeared to be a significant advantage of the multiple SISO approach did not appear to be particularly important in the numerical examples studied in this chapter. Both methods can also be adapted to

make use of a compensator that includes, besides the FIR design, an IIR compensator that inverts all invertible poles and zeros inside the unit circle. Both methods are capable of designing an MIMO repetitive controller that has quite fast, well behaved monotonic convergence to zero tracking error.

6.4 Experiment Design Using ILC for Parameter Identification

The use of iterative learning control was suggested in reference [30] as a method of experiment design for purposes of system identification. A phase cancellation ILC design was studied as a method to pull unmodeled residual modes or parasitic poles out of the noise in the data as ILC iterations progress, and then using the resulting data for identification. Normally one picks ILC laws that are intentionally made as robust as possible to model error. But in Chapter 5 we create ILC laws that are intentionally non-robust to model error, and then study their ability to identify parameter errors such as pole locations and damping factors. It is seen that the ILC law is very sensitive to phase errors in the model. But this sensitivity is often offset by a correlated change in the magnitude response, with the result that often the sensitivity is limited to model errors of a given sign. Hence, direct application of the methods can be very effective, but are not guaranteed to produce data that helps with the parameter identification. One can address this issue by modifying the nominal model parameters of interest, going both up and down in value, when designing the learning laws so that one of the two ILC iterations will result in the desired data. Of course the method will maintain the sensitivity to missing residual modes or poles that was demonstrated in the previous work.

References

1. T. Inoue, M. Nakano, and S. Iwai, "High Accuracy Control of a Proton Synchrotron Magnet Power Supply," *Proceedings of the 8th World Congress of IFAC*, Vol. XX, 1981, pp. 216-221.

2. S. Hara, and Y. Yamamoto, "Synthesis of Repetitive Control Systems and its Applications," *Proc. 24th IEEE Conference on Decision and Control*, 1985, pp. 326-327.

3. S. Hara, T. Omata, and M. Nakano, "Stability of Repetitive Control Systems," *Proceedings of the. 24th IEEE Conference on Decision and Control*, 1985, pp. 1387-1392.

4. R. H. Middleton, G. C. Goodwin, and R. W. Longman, "A Method for Improving the Dynamic Accuracy of a Robot Performing a Repetitive Task," University of Newcastle, Newcastle, Australia, EE Department Tech Report EE8546, 1985. Also, *International Journal of Robotics Research*, Vol. 8, 1989, pp. 67-74.

5. M. Tomizuka, T.-C. Tsao, and K. K. Chew, "Analysis and Synthesis of Discrete Time Repetitive Controllers," *Journal of Dynamic Systems, Measurement, and Control*, Vol. 111, 1989, pp. 353-358.

6. K. Åström, P. Hagander, and J. Strenby, "Zeros of Sampled Systems," *Proceedings of the Nineteenth IEEE Conference on Decision and Control*, 1980, pp. 1077-1081.

7. B. Panomruttanarug and R. W. Longman, "Repetitive Controller Design Using Optimization in the Frequency Domain," *Proceedings of the 2004 AIAA/AAS Astrodynamics Specialist Conference*, Providence, RI, August 2004.

8. R. W. Longman, "Iterative Learning Control and Repetitive Control for Engineering Practice," *International Journal of Control*, Special Issue on Iterative Learning Control, Vol. 73, No. 10, July 2000, pp. 930-954.

9. S. Songschon and R. W. Longman, "Comparison of the Stability Boundary and the Frequency Response Stability Condition in Learning and Repetitive Control," *International Journal of Applied Mathematics and Computer Science*, Vol. 13, No. 2, 2003, pp. 169-177.

10. R. W. Longman, K. Xu, and M. Q. Phan, "Design of Repetitive Controllers in the Frequency Domain for Multi-Input Multi-Output Systems," *Advances in the Astronautical Sciences*, Vol. 129, 2008, pp. 1593-1612.

11. J. W. Yeol, R. W. Longman, and Y. S. Ryu, "On the Settling Time in Repetitive Control Systems," *Proceedings of the 17th IFAC World Congress*, Seoul, Korea, July 2008.

12. B. Panomruttanarug and R. W. Longman, "Designing Optimized FIR Repetitive Controllers from Noisy Frequency Response Data," *Advances in the Astronautical Sciences*, Vol. 127, 2007, pp. 1723-1742.

13. K. Xu and R. W. Longman, "Use of Taylor Expansions of the Inverse Model to Design FIR Repetitive Controllers." *Advances in the Astronautical Sciences*. Vol. 134, 2009, pp. 1073-1088.

14. B. Panomruttanarug and R. W. Longman, "Frequency Based Optimal Design of FIR Zero-Phase Filters and Compensators for Robust Repetitive Control," *Advances in the Astronautical Sciences*, Vol. 123, 2006, pp. 219-238.

15. J. Bao and R. W. Longman, "Enhancements of Repetitive Control using Specialized FIR Zero-Phase Filter Designs," *Advances in the Astronautical Sciences*, Vol. 129, 2008, pp. 1413-1432.

16. S. C. Lee, M. Q. Phan, and R. W. Longman, "Multiple-Model Design of Robustified Repetitive Controllers with Optimized Convergence Rate," *Proceedings of the 2006 AIAA Guidance, Navigation, and Control Conference*, Keystone, CO, Aug. 2006.

17. W. Kang and R. W. Longman, "The Effect of Interpolation on Stability and Performance in Repetitive Control," *Advances in the Astronautical Sciences*, Vol. 123, 2006, pp. 1163-1182.

18. R. W. Longman, J. W. Yeol, and Y. S. Ryu, "Improved Methods to Cancel Multiple Unrelated Periodic Disturbances by Repetitive Control," *Advances in the Astronautical Sciences*, Vol. 123, 2006, pp. 199-218.

19. R. W. Longman, J. W. Yeol, and Y. S. Ryu, "Tuning and Performance of Robust Multiple-Period Repetitive Control," *Advances in the Astronautical Sciences*, Vol. 124, 2006, pp. 687-705.

20. M. Yamada, Z. Riadh, and Y. Funahashi, "Design of Robust Repetitive Control System for Multiple Periods," *Proceedings of the 39th IEEE Conference on Decision and Control*, 2000, pp. 3739-3744.

21. M. Yamada, Z. Riadh, and Y. Funahashi, "Discrete-Time Repetitive Control Systems with Multiple Periods," *Proceedings of 6th International Workshop on Advanced Motion Control*, 2000, pp. 228-233.

22. S. G. Edwards, B. N. Agrawal, M. Q. Phan, and R. W. Longman, "Disturbance Identification and Rejection Experiments on an Ultra Quiet Platform," *Advances in the Astronautical Sciences*, Vol. 103, 1999, pp. 633-651.

23. H.-J. Chen, B. N. Agrawal, R. W. Longman, and M. Q. Phan, "Frequency-Domain Clear-Box Disturbance Rejection," *Advances in the Astronautical Sciences*, Vol. 105, 2000, pp. 73-92.

24. H. M. Brown, M. Q. Phan, S. C. Lee, and R. W. Longman, "Robustified Repetitive Controllers with Monotonic Convergence for Multiple-Input Multiple-Output Systems," *Advances in the Astronautical Sciences*, Vol. 129, 2008, pp. 1893-1912.

25. R. W. Longman, "On the Theory and Design of Linear Repetitive Control Systems." *European Journal of Control*. Special Section on Iterative Learning Control, Guest Editor Hyo-Sung Ahn, Vol. 16, No. 5, 2010, pp. 447-496.

26. R. W. Longman, J.-N. Juang, M. Q. Phan, and K. Xu, "On Multi-Input Multi-Output Repetitive Control Design Methods." *Advances in the Astronautical Sciences*, 2012, to appear.

27. G. C. Goodwin, R. Payne, "Dynamic System Identification, Experiment Design, and Data Analysis. Chapter 6, Experiment Design." 1977, Academic Press, NY.

28. I. Bauer, H. G. Bock, S. Körkel, and J. P. Schlöder, "Numerical Methods for Optimum Experimental Design in DAE Systems." *Journal of Computational and Applied Mathematics*, Vol 120, 2000, pp. 1-25.

29. S. Körkel, E. Kostina, H. G. Bock, and J. P. Schlöder, "Numerical Experiments for Nonlinear Dynamic Processes." *Optimization Methods and Software Journal*, Vol 19, No. 3-4, 2004, pp. 327-338.

30. R. W. Longman, and M. Q. Phan, "Iterative Learning Control as a Method of Experiment Design for Improved System Identification." Special Issue on Parameter Estimation and Experiment Design. *Optimization Methods and Software Journal*, Taylor and Francis Publishers, Vol. 21, No. 6, Dec. 2006, pp. 919-941.

31. K. L. Moore, J.-X. Xu, Guest Editors, "Special Issue on Iterative Learning Control." *International Journal of Control*, Vol. 73, No. 10, July 2000.

32. Z. Bien, J.-X. Xu, Editors, "Iterative Learning Control: Analysis, Design, Integration and Applications." Kluwer Academic Publishers, Boston, 1998.

33. R. W. Longman, "Designing Iterative Learning and Repetitive Controllers." *Iterative Learning Control: Analysis, Design, Integration and Applications.* Bien, J.-X. Xu editors, pp.107-146. Kluwer Academic Publishers, Boston, 1998.

34. H. Elci, R. W. Longman, M. Q. Phan, J.-N. Juang, and R. Ugoletti, "Automated Learning Control through Model Updating for Precision Motion Control." *Adaptive Structures and Composite Materials: Analysis and Applications, ASME*, AD-Vol. 45/MD-Vol. 54, 1994, pp. 299-314.

35. R. W. Longman, and Y.-C. Huang, "The Phenomenon of Apparent Convergence Followed by Divergence in Learning and Repetitive Control." *Intelligent Automation and Soft Computing*, Special Issue on Learning and Repetitive Control, Guest Editor: H. S. M. Beigi, Vol. 8, No. 2, 2002, pp. 107-128.

36. J.-N. Juang, M. Q. Phan, L. G. Horta, and R. W. Longman, "Identification of Observer/Kalman Filter Markov Parameters: Theory and Experiments." *Journal of Guidance, Control, and Dynamics*, Vol. 16, No. 2, 1993, pp. 320-329.

37. J.-N. Juang, *Applied System Identification*. 1994, Prentice Hall, Englewood Cliffs, NJ.

38. P. Van Overschee, and B. De Moor, *Subspace Identification for Linear Systems: Theory, Implementation, and Applications*. 1996, Kluwer Academic Publishers, Boston.

39. R. W. Longman, K. Xu, and B. Panomruttanarug, "Designing Learning Control that Is Close to Instability for Improved Parameter Identification." *Modeling, Simulation and Optimization of Complex Processes*, Bock, Kostina, Phu, and Rannacher Editors, Springer-Verlag, Heidelberg, 2008, pp. 359-370.

40. Y.-C. Huang and R. W. Longman, "The Source of the often Observed Property of Initial Convergence Followed by Divergence in Learning and Repetitive Control," *Advances in the Atronautical Sciences*, Vol. 90, 1996, pp. 555-572.

41. K. Chen, R. W. Longman, and M. Q. Phan, "On the Relationship Between Repetitive Control and Model Predictive Control," *Proceedings of the 2006 AIAA/AAS Astrodynamics Specialist Conference*, Keystone, CO, Aug. 2006.

42. J. W. Yeol and R. W. Longman, "Time and Frequency Domain Evaluation of Settling Time in Repetitive Control." *Proceedings of the AIAA/AAS Astrodynamics Specialist Conference*. Hawaii, August 2008.